Journal of Cultural Heritage 44 (2020) 63–82

Available online at ScienceDirect www.sciencedirect.com

Elsevier Masson France EM|consulte www.em-consulte.com/en

Original article

Technological transfers in the Mediterranean on the verge of Romanization: Insights from the waterproofing renders of Nora (Sardinia, Italy)

Michele Secco[a,b,*], Simone Dilaria[a], Jacopo Bonetto[a], Anna Addis[c], Sergio Tamburini[d], Nereo Preto[e], Giulia Ricci[b,e], Gilberto Artioli[b,e]

[a] University of Padova, Department of Cultural Heritage (DBC), Italy
[b] University of Padova, Inter-Departmental Research Center for the Study of Cement Materials and Hydraulic Binders (CIRCe), Italy
[c] Bruker Daltonics S.r.L., Italy
[d] National Research Council, Institute of Condensed Matter Chemistry and Technologies for Energy (CNR-ICMATE), Italy
[e] University of Padova, Department of Geosciences, Italy

ARTICLE INFO

Article history:
Received 23 August 2019
Accepted 16 January 2020
Available online 10 February 2020

Keywords:
Nora
Punic and Roman mortars and renders
Pozzolanic reaction
Magnesium-silicate-hydrate (M-S-H)
Rietveld quantitative phase analysis
Nuclear magnetic resonance

ABSTRACT

The paper reports the results of a multi-analytical characterization study on the renders constituting the waterproofing coatings of 11 cisterns located in the Punic-Roman archaeological site of Nora (Southern Sardinia, Italy). The multi-layer layout of the coatings is related both to the practice of putting several strata of render in a synchronic plastering phase, and to frequent restoration activities related to the prolonged use of the cisterns. The aims of this study are (a) to determine the compositional and textural properties of the binding materials, (b) to define the coating systems employed in diachronic plastering phases, and (c) to identify the role of diverse cultural influences in the modification of the render recipes along time. The combined interpretation of the results obtained through petrographic, mineralogical, microstructural and microchemical analyses allowed discriminating different render types employing various pozzolanic additives, whose utilization is related both to Punic and Roman technological practices. Furthermore, the cementation processes of the renders were studied through an in-detail mineralogical and spectroscopic characterization of their binder fractions. The results demonstrated that hydraulic reactions were often enhanced through specific treatments of the binding mixtures, such as the combined use of different pozzolanic additives, the adoption of comminution processes to increase their reactive specific surface and the use of saltwater to enhance silica and alumina activity in solution through pH increase. Such technological practices promoted in some cases not only the precipitation of Ca-based pozzolanic reaction products (C-S-H and AFm phases), but also the formation of nanostructured anthropogenic magnesium-silicate-hydrate (M-S-H) phyllosilicate gels, leading to a further increase of the cohesive properties of the binding mixtures. A combined interpretation of the results with the cistern construction chronologies confirmed that cistern coating techniques in Nora were still largely influenced by Punic traditions even two centuries after the Roman conquest of Sardinia.

1. Introduction

The ancient city of Nora is located on a peninsula in the southern edge of the Gulf of Cagliari, Sardinia. The site is arranged around three small andesite mounds surrounded by arenite sedimentary outcrops [1]. Nora's cape was occupied by human settlements since the late Bronze age, as demonstrated by the presence of Sardinian Nuragic pottery. During the 8th century B.C.E., the area became one of the main Phoenician Sardinian harbors and a port of trade of the Levantine merchants (*emporium*) for the exchange of goods (mainly metals) with inland populations. The Phoenician settlement is testified by a series of postholes for wooden huts and by a necropolis recently discovered in the northern part of the peninsula [2], while the development of a first stable urban settlement dates back to the end of the 6th century B.C.E., when Nora and the whole Sardinia were taken over by Carthage. Punic population, transferred from Africa for the agricultural exploitation of the

* Corresponding author at: University of Padova, Department of Cultural Heritage (DBC), Italy.
E-mail address: michele.secco@unipd.it (M. Secco).

https://doi.org/10.1016/j.culher.2020.01.010
1296-2074/

countryside, built a quartered town, with streets, sanctuaries, stone buildings [3] and two hypogeal chambered necropolises [1,4,5]. In 238 B.C.E., after the First Punic War, Sardinia was conquered by Rome and Nora was gradually refurbished (not earlier than the 1st century B.C.E.) by Roman structures such as a wide forum, temples, baths and a theatre, despite being still culturally and socially influenced by the Punic culture. Such urban development reached its peak during the 3rd century C.E. In the late 4th century C.E., the construction of a Christian Basilica in the western part of the city indicated the spread of Christianity, while a steep socio-economic decline took place from the 5th until the 7th century C.E. [1]. The site, probably abandoned by the end of the 8th century C.E., was progressively obliterated by the anthropic and geological evolutions of the area, until the end of the 19th century, when the first portions of the city were discovered by F. Vivanet and G. Patroni. The first great archaeological excavations were promoted between 1952 and 1960 by the supervisor of Sardinian Antiquities Gennaro Pesce [1].

In recent decades, the Superintendence for Archaeological Heritage of the provinces of Cagliari and Oristano coordinated systematic archaeological missions in collaboration with several Academic institutions (University of Padova, Milan, Genoa, Cagliari, Viterbo), in order to improve the knowledge of the ancient city [6]. One of the peculiarities of the Punic and Roman phases of Nora is the presence of several cisterns for the collection of rainwater, as proved by the works of the recent excavation campaigns, which led to the identification of 92 man-made water reservoirs [7]. The pervasive presence of cisterns in Nora depends on the fact that the first aqueducts in Sardinia were built only from the Augustan age on, and they were still inadequately distributed throughout the island, at least until the Severian age. Nora had its aqueduct only in the 3rd century C.E., having used only wells and cisterns to fulfil its water needs for the first seven centuries of its life.

2. Aim of the research

Recent in situ macroscopic investigations indicated that Nora cisterns are characterized by the presence of coating systems constituted of several render layers, which were placed not only after the construction of the structures, but also during different, and frequent, re-plastering activities.

The aim of this study is to recognize and parametrize the coating phases of the cisterns, to understand if render recipes varied along times, if Punic technological traditions were maintained after Sardinia was declared Roman province (227 B.C.E.) and how Roman and Punic cultures influenced each other.

3. Materials and methods

3.1. Materials

On the basis of the analysis conducted by S. Cespa on the structural characteristics and distribution of 92 cisterns unearthed in Nora [7], followed by a preliminary petrographic examination of the render coatings [8], this study was focused on 11 significant cisterns distributed in different areas of the ancient city. Both cisterns with reliable construction chronologies and undated cisterns excavated in past decades without stratigraphic methodologies were included in the research. The different geometric layouts of the cisterns, reflecting construction techniques and morphologies frequently occurring in Punic-Roman sites of Sardinia [7–10], were also taken into account in the selection process. The analyzed cistern typologies, labeled in accordance with Cespa enumeration [7], are reported hereafter:

a) Rock-grave cisterns (C28, C36, C92). This typology was made by coating with renders the chambers of former Punic rock-graves dug within arenite outcrops (Fig. 1a). Such change of use occurred presumably in Roman times. The original entrance pits of the tombs were used as wells, apart from one structure (C92), where a secondary rectangular well was dug and coated with render after the change of use. The size of these structures is highly variable, and is correlated to the layout of the former Punic graves.
b) Bathtub cisterns (C2, C4, C5, C7, C8, C13, C91). This type of cistern is an elongated trench with semi-cylindrical terminations, conferring the peculiar bathtub-like shape (Fig. 1b, c, d). This typology is widely diffused in Carthaginian territories and is linked to Punic building traditions. Such morphology was frequently adopted in Sardinia, also in structures built during the Roman period. The length of these structures ranges between 2.5 and 8.5 m, their width is comprised between 1 and 1.5 m, while their depth can reach 4 m.
c) Rectangular cisterns (C29). This type of cistern is characterized by an elongated rectangular plan, uncommon for Punic building traditions (Fig. 1e). The analyzed structure has a length of 10.5 m, a width of 1.26 m and a depth of 1.95 m.

Samples were collected by means of hammers and chisels from the constituting elements of the cisterns, namely walls (I) and floors (F). As previously reported, wall render samples are often stratified in several layers, owing both to the multi-layer layout of synchronic coating systems and to diachronic re-plastering operations: they were subdivided according to the relevant hypothesized coating system and labeled with progressive letters. Furthermore, the sample for the render of the secondary rectangular well of C92 was labeled as C92-Iw.

The analytical plan was organized in three progressive steps described in the following paragraphs, to broaden the knowledge on application procedures, composition, and properties of the binding mixes.

3.2. Methods

3.2.1. Micro-stratigraphic characterization of the coating systems

Samples representing the entire stratigraphy of coating layers were investigated in order to parametrize the morphologies of layer interfaces and distinguish rough preparation strata from smoothed finishing surfaces, defining the occurrence of several diachronic plastering phases. The study was performed by means of confocal laser scanning microscopy (CLSM), using an Olympus LEXT OLS4100 laser scanning digital microscope. Several stitched images for each sample were acquired employing simultaneously optical and laser light.

3.2.2. Multi-analytical characterization of the render typologies

All the samples were subject to a preliminary petrographic study to cluster the renders of the coating systems according to their composition. The study was performed following the macroscopic and microstratigraphic analytical procedures for the study of mortar-based building materials described in Standard UNI 11176:2006 “Cultural heritage - Petrographic description of a mortar”. Mass color was defined through Munsell soil color charts [11]. The study was performed through macroscopic and stereomicroscope observations, and by transmitted light optical microscopy (TL-OM) on 30 μm thin sections, obtained by vacuum impregnating portions of the materials with epoxy resin and sectioning them transversally. The microscopic study was performed on a Nikon Eclipse ME600 microscope. Binder to aggregate ratios and porosity percentages have been estimated qualitatively by means of image analysis of thin sections [12], while the cohesion of the materi-

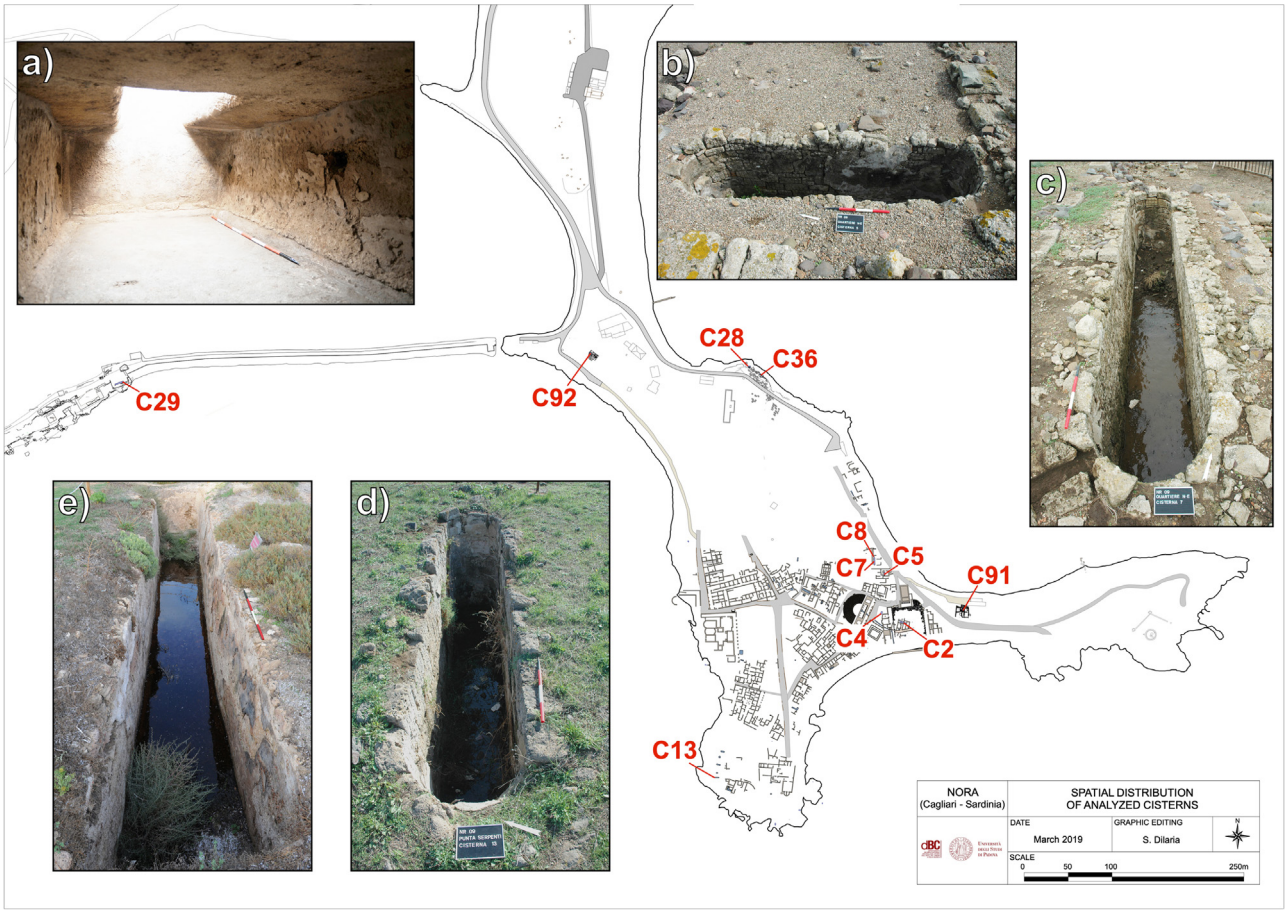

Fig. 1. Map with the spatial distribution of the analyzed cisterns within the Nora archaeological site, and photographs of the different morphologies of the water systems: a) rock-grave cistern (C92); b, c, d) bathtub cisterns (C5, C7 and C13, respectively); e) rectangular cistern (C29). Each band of the ranging rods measures 20 cm. Pictures taken by S. Dilaria and S. Cespa.

als has been qualitatively evaluated according to the resistance to hand crushing, as prescribed by the above-mentioned Standard.

Then, a selection of render samples – representative for each petrographic group – was subject to a detailed mineralogical, microstructural and microchemical characterization to better define their compositional properties. Mineralogical analyses of the bulk samples were performed by quantitative phase analysis based on X-ray powder diffraction data (XRPD-QPA). The materials were subject to micronization by a McCrone mill, using a plastic jar with agate grinding elements and ethanol 99% as micronizing fluid. Furthermore, 20 wt% of ZnO was added to the powders for the quantification of the paracrystalline fraction through the internal standard method. Data were collected using a Bragg–Brentano θ–θ diffractometer (PANalytical X'Pert PRO, Co Kα radiation, 40 kV and 40 mA) equipped with a real-time multiple strip (RTMS) detector (X'Celerator by Panalytical). Data acquisition was performed by operating a continuous scan in the range 3–85 [°2θ], with a virtual step scan of 0.02 [°2θ]. Diffraction patterns were interpreted using the X'Pert HighScore Plus 3.0 software by PANalytical, qualitatively reconstructing mineral profiles of the compounds by comparison with PDF databases from the International Centre for Diffraction Data (ICDD). Then, QPAs were performed using the Rietveld method [13]. Refinements were accomplished with BGMN-Profex software (version 3.12.1) [14,15]. The observed Bragg peaks in the powder patterns were modelled through a pseudo-Voigt function, fitting the background by a 12-coefficients Chebyshev polynomial. For each phase, the lattice parameters, Lorentzian crystal sizes and scale factors were refined. Although samples were prepared with the back-loading technique to minimize preferred orientation of crystallites *a priori*, any residual preferred orientation effect was modelled during the refinement with the March Dollase algorithm [16]. The starting structural models for the refinements were taken from the International Crystal Structure Database (ICSD). Furthermore, a Rietveld-compatible procedure was adopted to quantify the amount of nanocrystalline phyllosilicate gels in the analyzed samples. Such phases are characterized by structural disorder issues such as short range stacking order and turbostratic disorder [17], and thus they were quantified by modeling the turbostratic disorder according to the "single layer approach" [18] on a cis-vacant 2:1 layer dioctahedral smectite structure included in the software package [19].

Finally, the thin sections of selected samples were microstructurally and microchemically characterized by scanning electron microscopy and energy-dispersive microanalysis (SEM-EDS). A CamScan MX2500 scanning electron microscope has been used, equipped with a LaB_6 cathode and a four-quadrant solid state BSE detector for imaging. The analytical conditions were: accelerating voltage 20 kV; filament current 1.80 A; emission current 20 μA; aperture current 300 nA; working distance 20–30 mm. Furthermore, an EDAX-EDS energy dispersive X-rays fluorescence spectrometer was used for chemical microanalysis, mounting a Sapphire Detector composed by a LEAP + Si(Li) crystal and a Super Ultra-Thin Window. Qualitative interpretation of spectra and semi-quantitative chemical analysis were performed through SEM Quant Phizaf software.

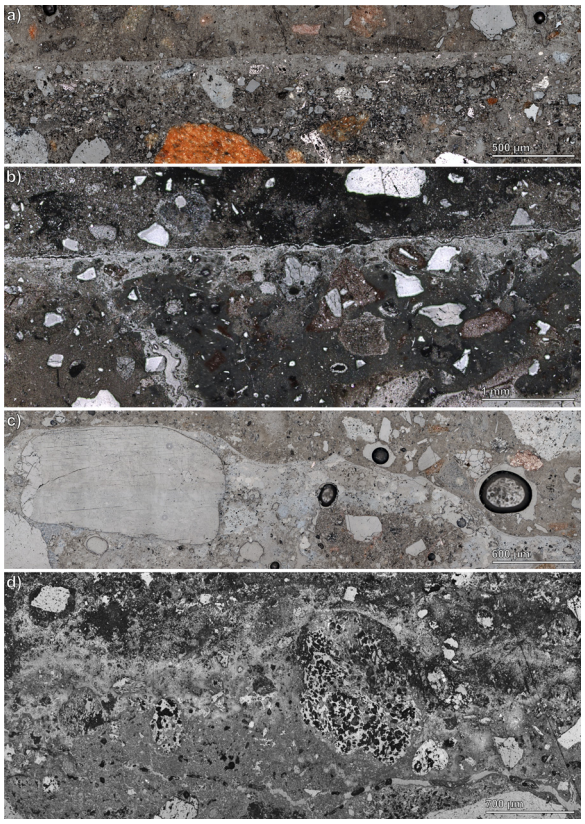

Fig. 2. CLSM micrographs representative of the interfacial characteristics of the render layers in the Nora cisterns: a, b) typical interfaces for diachronic render layers (C7_I1.b/C7_I2.a and C13_I2.a/C13_I3.a, respectively); c, d) typical interfaces for synchronic render layers (C29_I1.b/C29_I1.c and C4_I2.b/C4_I2.c, respectively).

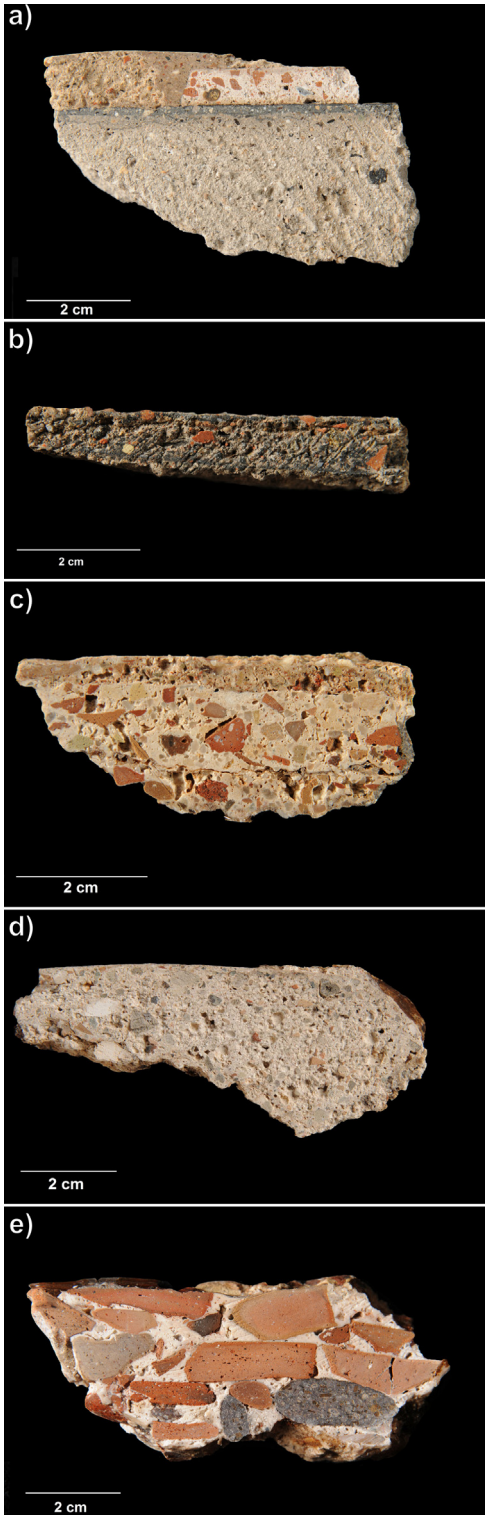

Fig. 3. Cross-sections of representative samples for each render/concrete typology applied in the Nora cisterns: a) C13_I1a, b (ASH, below); b) C2_I1.b (ASH-CP); c) C29_I1.a, b, c (CP); d) C91_I1.b (PUM-CP); e) C36-F1 (CCC).

3.2.3. Mineralogical and spectroscopic characterization of the binder fractions

The multi-analytical characterization of the renders constituting the coating systems was complemented with a combined mineralogical-spectroscopic study of their binder fractions, to determine the reactivity properties of the employed binding mixtures and the extent of the pozzolanic reaction processes.

The study was performed on binder-concentrated samples obtained following the Cryo2Sonic 2.0 separation procedure [20], custom-modified through the addition of a chelating agent to the sedimentation solution (sodium hexametaphosphate 0.5% wt.) to favor the suspension of the finer, non-carbonate phases such as clay minerals and pozzolanic products, prone to flocculation due to their surface charges. After the extraction, the ultrafine powders were mineralogically characterized through XRPD-QPA, adopting the same analytical protocol used for the analysis of the bulk samples, and implementing further treatments to better discriminate the nature of the paracrystalline fraction. More in detail, representative fractions of the binder-concentrated samples were weighed with an analytical microbalance, treated with acetic acid for the removal of carbonates and other acid-soluble phases according to the procedure described in [21] and the residues were weighed again to determine the amount of dissolved fraction and analyzed through XRPD-QPA. Then, by comparing the weights and the quantitative profiles before and after the acid treatment, both soluble and insoluble paracrystalline fractions for each sample were quantified. Furthermore, the Total Organic Carbon (TOC) and the stable isotopic composition of carbon ($\delta^{13}C$) of selected samples were simultaneously determined. Approximately 2 mg of powder for each sample were weighed with an analytical microbalance in silver cups and treated repeatedly with HCl (9%) on a hot (65 °C) plate, to remove carbonate and acid-soluble minerals, until the reaction was complete. The cups were then wrapped and analyzed for their C content with a Thermo Scientific Flash 2000 Elemental Analyzer, along with blanks and standards (pure marble, weighed at least 6

times between 0.1 and 1 mg). The obtained C contents were interpreted as the amount of organic carbon (i.e. charcoal) within each analyzed sample. The CO_2 developed in the Elemental Analyzer was transferred to a Thermo Delta V Advantage Isotopic Ratio Mass Spectrometer for the determination of $\delta^{13}C$. The measured $\delta^{13}C$ was normalized to the standard VPDB scale through an internal standard (Carrara marble), whose isotopic composition is periodically checked internally against the international standard NBS 19. The reproducibility of analyses normalized with this method, estimated by repeated analyses of an independent standard (C3 plant sucrose) treated identically to the analyzed samples, is 0.3‰ (1 s.d.).

Finally, the coordination and degree of polymerization of silicates and aluminates in the binder fractions of the render samples were studied through ^{29}Si and ^{27}Al Magic-Angle Spinning Solid-State Nuclear Magnetic Resonance (MAS-SSNMR). ^{29}Si and ^{27}Al spectra were collected on a Bruker AVANCE III 300 spectrometer, operating with a magnetic field of 7.0 T corresponding to ^{29}Si and ^{27}Al Larmor frequencies of 59.623 and 78.066 MHz, respectively, and equipped for solid-state analysis in 4 mm diameter zirconia rotors with Kel-F caps. The magic angle was accurately adjusted prior to data acquisition using KBr. ^{29}Si chemical shifts were externally referenced to solid tetrakis(trimetylsilyl)silane at −9.0 ppm (in relation to TMS) and ^{27}Al chemical shifts were externally referenced to $NaAlO_2$ (79.3 ppm). The quantitative ^{29}Si single-pulse experiments were collected at a spinning frequency of 6 kHz, a recycling delay of 100 s and 2000 transients. ^{27}Al experiments were collected at a spinning frequency of 13 kHz with a recycle time of 2 s. The signal patterns of the spectra were deconvoluted with the Peak Analyzer routine of Origin Pro 2018 software, using combined Gaussian-Lorentzian peak functions commonly employed for the fit of NMR data [22].

4. Results

4.1. Micro-stratigraphic characterization of the coating systems

Confocal analyses of sample layer interfaces, coupled with *in situ* analyses of surface coating treatments for all the cisterns examined, were crucial to identify the coating systems and confirm the hypothesized coating phases (Table 1), distinguishing between preparation wall renders and finishing ones. This was a fundamental step to chronologically distinguish plastering and re-plastering activities and to identify plastering techniques adopted by Nora artisans.

Finishing layers present a straight profile and the lime carbonation skin, particularly pronounced for fat renders, is usually evident (130–200 μm) due to the prolonged exposure of the surface to the air (Fig. 2a, b). Sometimes, finishing surfaces are refined with a thin layer of pure lime, 200–500 μm thick. Macroscopically, finishing surfaces are extremely well polished. In occasion of repair procedures, the external render layers have been frequently pattered by the use of chisels to improve the adhesion of new coatings. The identification of these incisions is a useful tool to discriminate different coating phases.

Preparation layers, on the other hand, present a corrugated profile, carbonation is either not present or poorly visible and sometimes aggregate particles are shared between two superimposed layers (Fig. 2c, d). Macroscopically, preparatory layers are characterized by rough superficial textures.

In this way, wall render samples, collected with the entire layer stratigraphy, were subsequently distinguished according to separate plastering phases, related to both construction and restoration activities. Coating systems are constituted by 1 up to 4 layers for each plastering phase (Fig. 10).

4.2. Multi-analytical characterization of the render typologies

Based on the results obtained by TL-OM, XRPD-QPA and SEM-EDS, the wall render layers have been clustered into five types, while all the concrete-like floors were clustered within an additional type (Table 1). The main characteristics of each type are reported hereafter. A strict terminology has been applied for the macroscopic categorization of the render and concretes layers, based on the lexicon adopted in the archaeological literature [23,24].

a) *Ash renders (ASH).* Such renders are present only in the first coating systems of C5 and C13 cisterns, both as centimetric base layers and millimetric finishing ones. They are macroscopically characterized by grey to very dark bluish-grey colors (5B-3/1) and moderate cohesion (Fig. 3a). Binder to aggregate (B/A) ratios are typical for fat renders, and the aggregate fraction is mainly constituted by ash and charcoal derived from organic matter combustion, with a sporadic occurrence of natural sand (Fig. 4a).

The natural sand component presents a highly sorted unimodal granulometric distribution centered within the fine sands granulometric range [25], with dominant quartz grains and a secondary occurrence of andesite and sandstone clasts, feldspar crystals, micas and fine carbonate sand. Pyroxenes, amphiboles and opaque minerals are rare. Such constituents are fully compatible with the locally available sediments [26].

The anthropogenic aggregate component is made of texturally and compositionally heterogeneous ash clusters reaching, in some cases, dimensions of several hundred μm (Fig. 4a). They constitute the inorganic residue of organic matter combustion, associated to sporadic charcoal frustules often retaining the cellular shapes of wood (Fig. 4b). The ash clusters are constituted of matrices of cryptocrystalline particles (Fig. 5a), mainly siliceous-aluminous in composition with associated calcium, magnesium, phosphorous, alkalis, iron, chlorine and titanium (Fig. 5c1). Significant enrichments in calcium towards the interfacial portions with the surrounding binding matrices are often observed (Fig. 5c2), indicating pozzolanic reaction processes with the lime binder [27]. Furthermore, highly porous particles of hundreds of μm (Fig. 5b), mainly constituted of calcium and phosphorous (Fig. 5c3), are frequently embedded within the ash clusters. Their compositional and textural characteristics allow identifying them as bone residues and their presence suggests a co-combustion of animal and plant organic matter for the production of the additive [28]. Finally, euhedral and subhedral silicate crystals are sporadically present and likely related to contaminations with local sediments during the combustion process. Apart from the two main classes of aggregate constituents, scarce (<5 vol%) fractions of crushed ceramics are present, whose occurrence is probably involuntary.

The binding matrices are mainly made of optically-extinct clusters of cryptocrystalline particles (Fig. 4a, 7a), fairly homogeneous in composition, with dominant calcium and an associated elemental profile similar to the cryptocrystalline ash components (Fig. 7b1, 7b2). Such characteristics indicate a composition given by anthropogenic calcite (i.e. formed after carbonation of the calcic binder) and finely powdered ash, possibly with hydration products of pozzolanic reaction processes between the lime binder and the additive [27]. Furthermore, diffuse lumps with dimensions from few to hundreds of μm are homogeneously distributed in the matrices (Fig. 7a). The typical TL-OM interference colors and the calcic composition indicate that they are composed of anthropogenic calcite. The analyzed samples are dense, with a volumetrically reduced pore network constituted of irregular vughs of few hundred μm, often related to the intrinsic porosity of the additive particles, and

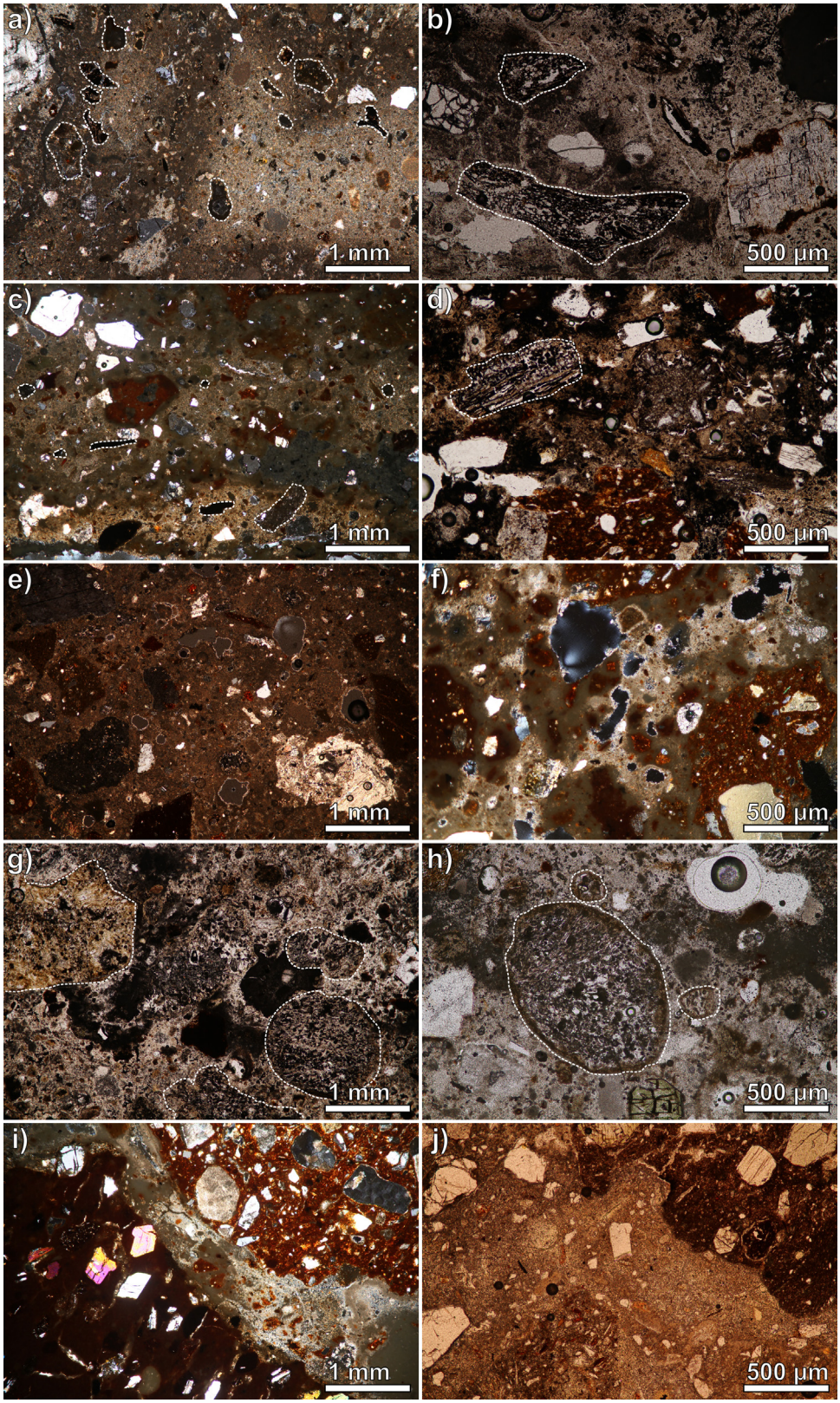

Fig. 4. TL-OM micrographs of representative samples for each render/concrete typology applied in the Nora cisterns. a) C13_I1.a (ASH), crossed polars (several optically extinct ash clusters are visible, the largest ones have been highlighted by dashed lines); b) C5_I1.a (ASH), plane polars (two charcoal frustules have been highlighted by dashed lines); c) C36_I2.a (ASH-CP), crossed polars (several optically extinct ash clusters are visible, the largest ones have been highlighted by dashed lines); d) C7_I1.b (ASH-CP), plane polars (a charcoal frustule has been highlighted by a dashed line); e) C29_I1.b (CP), crossed polars; f) C92_Iw (CP), crossed polars; g) C4_I2.a (PUM-CP), plane polars (pumice clasts have been highlighted by dashed lines) ; h) C91_I1.b (PUM-CP), plane polars (pumice clasts with evident reaction rims have been highlighted by dashed lines); i) C92_F1 (CCC), crossed polars; j) C91_F1 (CCC), plane polars.

Table 1
List of the analyzed cisterns, together with their typology, hypothesized chronology, architectural element of pertinence for the render/concrete samples, sequence of the coating phases and of the render layering, and analytical techniques employed for the characterization of the materials.

Cistern	Typology	Chronology	Element	Sample	Layer	Render Type	Analytical techniques						
							TL-OM	CLSM	XRPD bulk	XRPD binder	SEM-EDS	TOC-δ13C	NMR
C2	Bathtub	150-75 B.C.E.	Wall	**_I1**	**.a**	ASH-CP	x	x					
					.b	ASH-CP	x	x	x		x	x	
C4	Bathtub		Wall	**_I1**	**.a**	ASH-CP	x				x		
			Wall	**_I2**	**.a**	PUM-CP	x	x					
					.b	PUM-CP	x	x					
					.c	PUM-CP	x	x					
C5	Bathtub		Wall	**_I1**	**.a**	ASH	x	x			x		
					.b	ASH-CP	x	x					
			Wall	**_I2**	**.a**	ASH-CP	x	x	x				
					.b	ASH-CP	x	x					
					.c	PUM-CP	x	x					
			Wall	**_I3**	**.a**	PUM-CP	x	x			x		
					.b	PUM-CP	x	x			x		
					.c	PUM-CP	x	x			x		
					.d	PUM-CP	x	x	x		x		
			Wall	**_I4**	**.a**	PUM-CP	x	x					
C7	Bathtub		Wall	**_I1**	**.a**	ASH-CP	x	x	x		x		
					.b	ASH-CP	x	x			x		
			Wall	**_I2**	**.a**	ASH-CP	x	x			x		
					.b	PUM-CP	x	x	x		x		
C8	Bathtub		Wall	**_I1**	**.a**	ASH-CP	x						
C13	Bathtub		Wall	**_I1**	**.a**	ASH	x	x	x	x	x	x	x
					.b	ASH	x	x			x		
			Wall	**_I2**	**.a**	CP	x	x			x		
			Wall	**_I3**	**.a**	CP	x	x	x		x		
C28	Rock-grave	Roman age	Wall	**_I1**	**.a**	ASH-CP	x	x					
			Wall	**_I2**	**.a**	ASH-CP	x	x			x		
					.b	ASH-CP	x	x	x	x	x	x	x
					.c	PUM-CP	x	x			x		
			Wall	**_I3**	**.a**	PUM-CP	x	x			x		
			Floor	**_F1**		CCC	x						
C29	Rectangular	Roman age	Wall	**_I1**	**.a**	CP	x	x			x		
					.b	CP	x	x	x	x	x		x
					.c	CP	x	x			x		
			Wall	**_I2**	**.a**	CP	x	x					
					.b	CP	x	x					
C36	Rock-grave	Roman age	Wall	**_I1**	**.a**	ASH-CP	x						
			Wall	**_I2**	**.a**	ASH-CP	x		x		x		
					.b	PUM-CP	x						
			Floor	**_F1**		CCC	x						
C91	Bathtub	1st-2nd century C.E.	Wall	**_I1**	**.a**	CP	x	x					
					.b	PUM-CP	x	x	x	x	x		x
					.c	PL	x	x			x		
			Floor	**_F1**		CCC	x						
C92	Rock-grave	2nd-1st century C.E.	Wall	**_I1**	**.a**	ASH-CP	x						
					.b	PL	x	x			x		
			Wall	**_I2**	**.a**	ASH-CP	x	x	x		x	x	
					.b	PL	x	x			x		
			Wall	**_I3**	**.a**	PUM-CP	x						
			Well wall	**_Iw**	**.a**	CP	x		x		x		
			Floor	**_F1**		CCC	x						

capillary micro-channels generated by the drying shrinkage of the setting render [29].

XRPD-QPA analyses (Table 2, Fig. 8a) showed a mineralogical composition consistent with the microscopic observation and given by dominant calcium carbonates, mainly anthropogenic, associated silicate phases of the aggregate fraction, and a relevant paracrystalline fraction related to the combustion residues and, possibly, to paracrystalline pozzolanic reaction products such as C-S-H and AFm phases, commonly characterized by the absence of crystal-like long-range ordering [27]. Furthermore, relevant amounts of crystalline AFm phase are present [30], formed after pozzolanic interactions between lime and the alumina component of the additive [31].

b) *Ash-cocciopesto renders (ASH-CP)*. This type was found in all the analyzed cisterns apart from C13, C29 and C91. Renders with such composition are present either as centimetric base layers or as millimetric finishing layers over ASH (C5) or other ASH-CP renders. They are macroscopically characterized by high cohesion and colors ranging from very dark bluish grey (5B-3/1) to pinkish grey (5YR-6/2) and light reddish brown (2.5YR-7/3) (Fig. 3b). B/A ratios are highly variable, and the aggregate fraction is constituted by an association of natural sand, combustion residues and crushed ceramics particles (Fig. 4c, d).

The natural sand fraction is compositionally affine to the one observed in the ASH renders, despite being present in higher amounts and with a slightly greater granulometric distribution centered within the fine sands [25]. The combustion residues are smaller with respect to the previous class and constituted by an association of ash clusters and charcoal particles (Fig. 4c, d). The ash clusters are almost exclusively made of porous cryptocrystalline matrices (Fig. 5e) with chemical profiles comparable to their counterparts within ASH renders, enriched in Al and Mg (Fig. 5f3),

Table 2
Mineralogical quantitative phase analysis of Nora cisterns' renders, obtained by full profile fitting of the experimental XRPD patterns according to the Rietveld method.

Sample	Type	Mineralogical composition (wt.%)															
		Calcite	Vaterite	AFm	Quartz	Albite	Orthoclase	Biotite	Sanidine	Analcime	Hematite	Illite/Muscovite	Ps-Gel	Clinochlore	Halite	Gypsum	Amorphous
C2_I1.b	ASH-CP	29.5	0.0	0.0	17.8	3.6	4.5	0.1	0.0	0.0	0.3	3.2	2.4	0.0	0.0	0.0	38.8
C5_I2.a	CP	65.7	0.0	0.0	6.3	1.6	1.7	0.4	0.0	0.0	0.4	2.6	0.0	0.0	0.4	0.0	20.8
C5_I3.d	PUM-CP	35.4	0.0	0.0	9.1	3.1	1.6	0.7	6.7	0.6	0.1	4.1	0.0	1.0	0.0	0.0	37.4
C7_I1.a	ASH-CP	43.9	0.0	0.0	9.8	2.4	4.2	0.4	0.0	0.0	0.3	2.1	2.4	0.0	0.0	0.0	34.6
C7_I2.b	PUM-CP	34.0	0.0	0.0	9.2	3.2	1.9	0.5	8.7	0.7	0.4	3.9	0.0	0.3	0.0	0.0	37.1
C13_I1.a	ASH	58.1	1.1	3.0	5.6	0.4	1.9	0.2	0.0	0.0	0.2	0.0	0.0	0.0	0.0	0.0	29.5
C13_I3.a	CP	45.6	0.0	0.0	10.8	1.9	2.9	0.4	0.0	0.0	0.5	2.6	0.0	0.0	4.1	0.8	30.4
C28_I2.b	ASH-CP	34.5	0.0	0.0	11.4	3.6	4.4	0.4	0.0	0.0	0.5	4.9	3.3	0.0	0.7	0.0	36.4
C29_I1.b	CP	45.9	0.7	0.0	18.8	2.6	5.0	0.2	0.0	0.0	0.2	3.0	0.0	0.1	0.0	0.0	23.6
C36_I2.a	ASH-CP	38.7	0.0	0.0	9.3	1.8	3.0	0.7	0.0	0.0	0.4	2.2	5.7	0.0	1.0	0.0	37.2
C91_I1.b	PUM-CP	42.3	1.3	0.0	6.4	2.2	3.4	0.7	5.2	0.5	0.0	2.4	0.0	0.8	0.0	0.0	34.9
C92_I2.a	ASH-CP	33.4	0.0	0.0	15.2	3.4	4.9	1.6	0.0	0.0	0.6	5.2	2.7	0.0	0.0	0.0	33.1
C92_Iw	CP	26.5	0.0	0.0	15.3	3.7	4.7	1.0	0.0	0.0	0.6	6.4	0.0	0.0	0.0	0.0	41.9

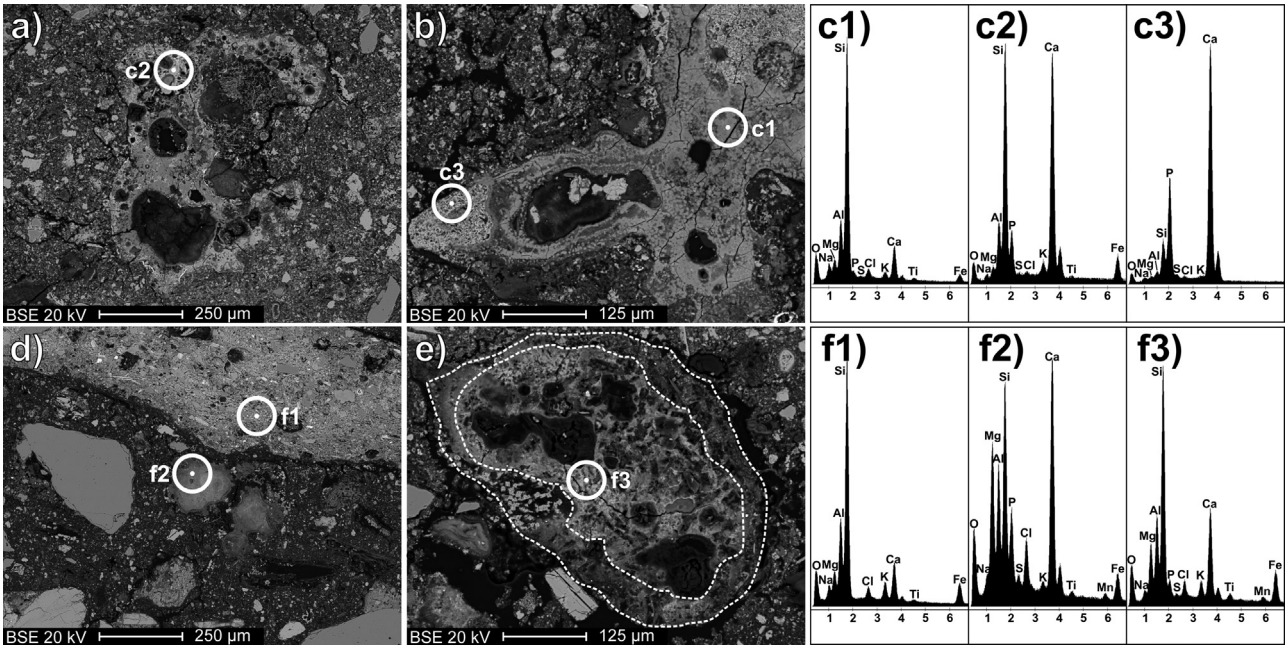

Fig. 5. a, b) Backscattered electrons images (BSI) of ash clusters within sample C13_I1.a, with indication of the spots of EDS analyses reported in figures c1, c2 and c3; d) BSI of a ceramic fragment and pozzolanic lumps and e) BSI of an ash cluster within sample C28_I2.b (the reaction rim has been highlighted by dashed lines), with indication of the spots of EDS analyses reported in figures f1, f2 and f3.

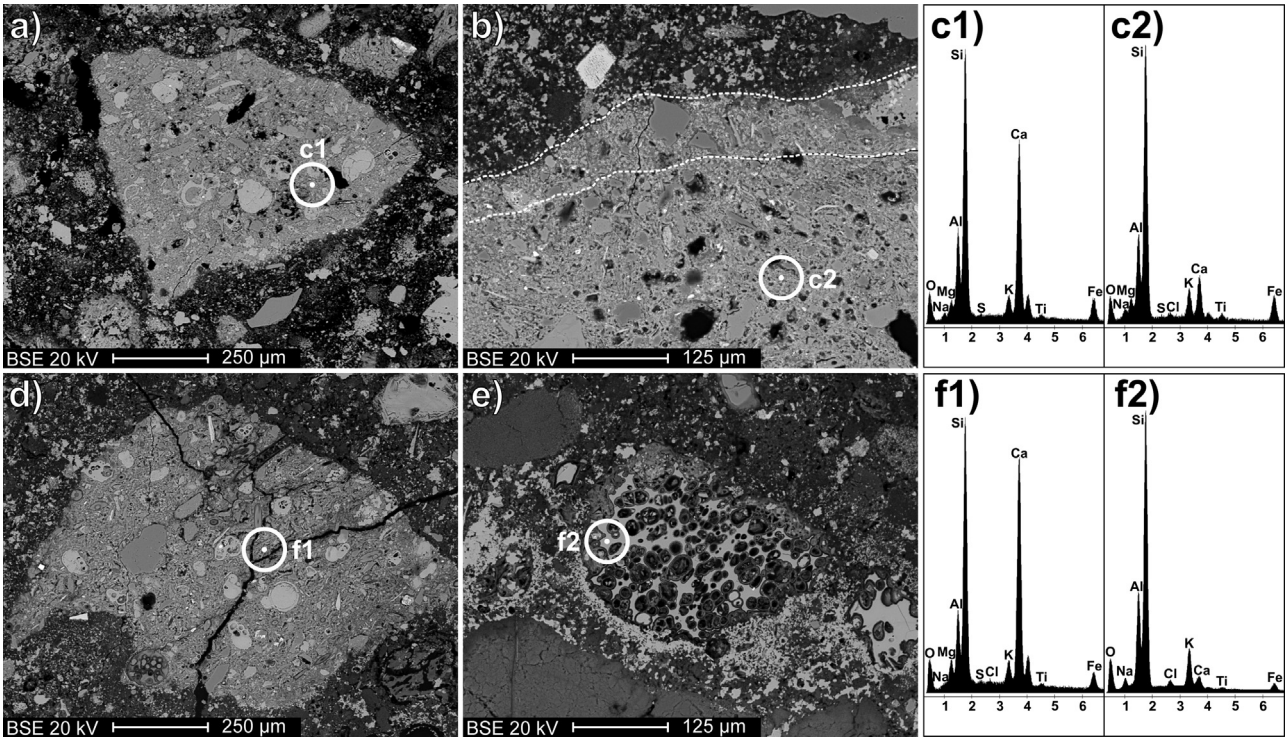

Fig. 6. a, b) BSI's of ceramic fragments within sample C29_I1.b (the reaction rim has been highlighted by dashed lines), with indication of the spots of EDS analyses reported in figures c1 and c2; d) BSI of a ceramic fragment and e) BSI of a pumice grain within sample C91_I1.b, with indication of the spots of EDS analyses reported in figures f1 and f2.

showing clear interfacial dissolution features related to pozzolanic reaction processes. The crushed ceramics particles are present within the samples in variable sizes and proportions, being sometimes abundant and with dimensions of several hundred µm, while in other cases they are smaller than 100 µm and more sporadic (Fig. 4c, d). Compositionally, they are constituted of highly vitrified siliceous-aluminous matrices (Fig. 5d), low in Ca (Fig. 5f1), with a silicate temper fraction affine to the natural sand aggregate within the renders. Interfacial pozzolanic reaction rims are always present.

The binding matrices are constituted of optically-extinct clusters of cryptocrystalline particles (Fig. 4c, 7c) rich in chemical elements compatible either with the cryptocrystalline ash components and the vitrified matrices of the crushed ceramics particles (Fig. 7d1, 7d2). Ca is the dominant chemical element in several

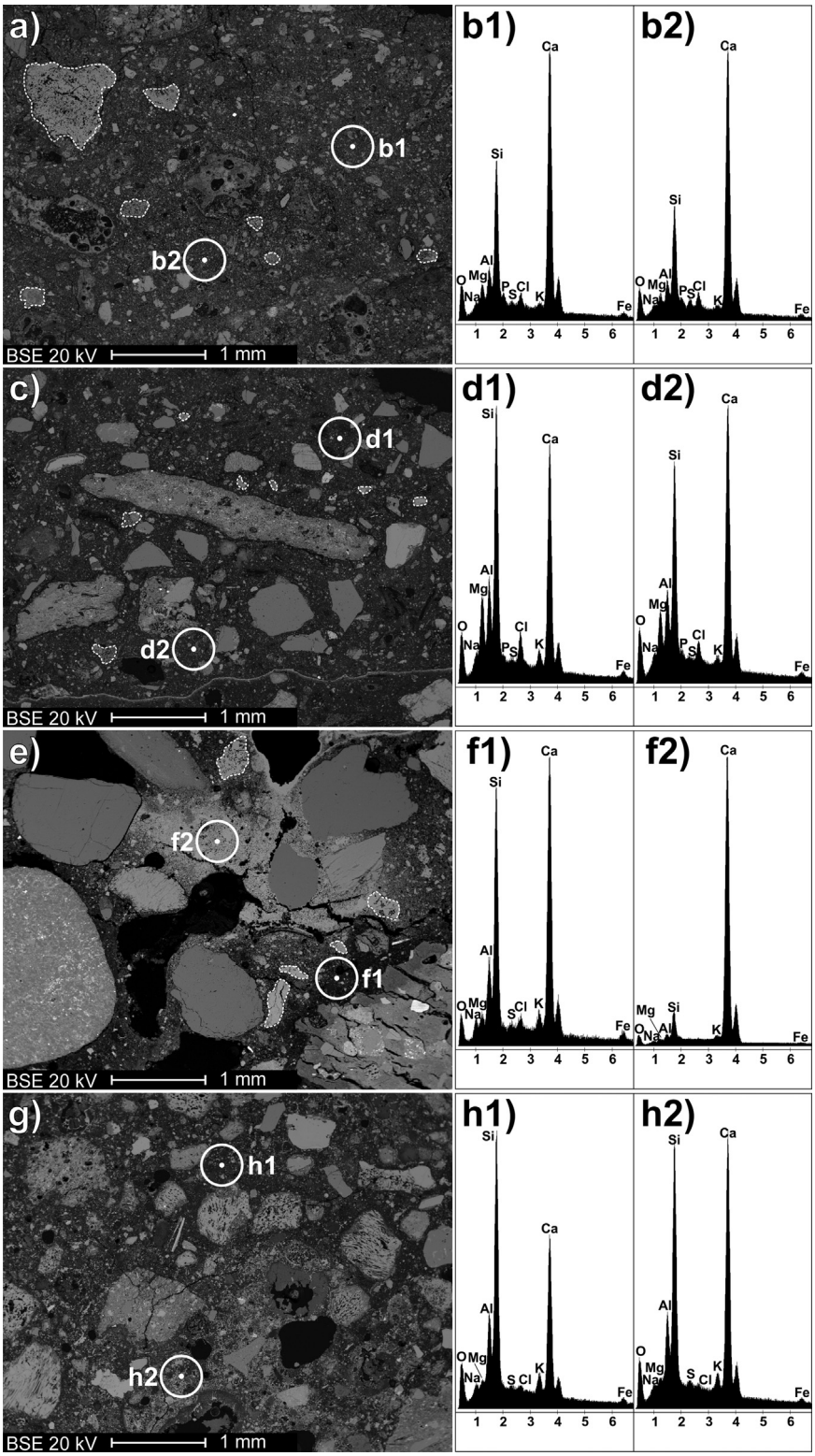

Fig. 7. a) BSI of sample C13_I1.a, with indication of the spots of EDS analyses of the binder matrices reported in figures b1 and b2 (several lumps are visible, the largest ones have been highlighted by dashed lines); c) BSI of sample C28_I2.b, with indication of the spots of EDS analyses of the binder matrices reported in figures d1 and d2 (several lumps are visible, the largest ones have been highlighted by dashed lines); e) BSI of sample C29_I1.b, with indication of the spots of EDS analyses of the binder matrices reported in figures f1 and f2 (several lumps are visible, the largest ones have been highlighted by dashed lines); g) BSI of sample C91_I1.b, with indication of the spots of EDS analyses of the binder matrices reported in figures h1 and h2.

areas, despite being often exceeded by Si. Furthermore, significant Mg, Al, Cl and Na enrichments are detectable. As observed in the previous class of renders, micrometer-sized lumps of anthropogenic calcite are present (Fig. 7c). Furthermore, several dense and homogeneous cryptocrystalline lumps with average dimensions of 100 μm are present (Fig. 5d). They are mainly silico-calcic in composition, with associated Mg, Al, P and Cl and minor amounts of Fe, alkalis, S, Ti and Mn (Fig. 5f2). Such evidence indicates a

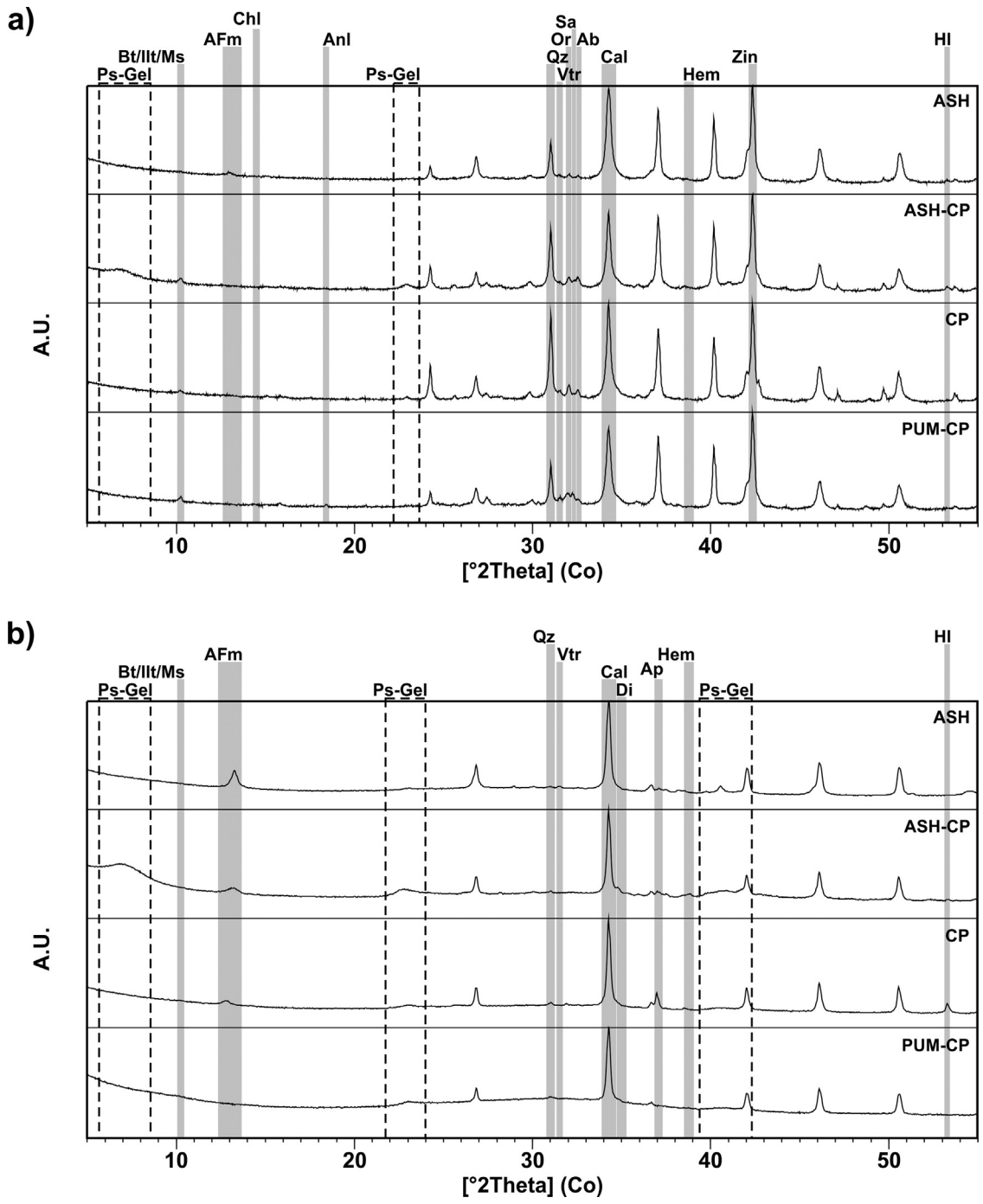

Fig. 8. XRPD patterns of representative samples for each render typology applied in the Nora cisterns (ASH: C13_I1.a; ASH-CP: C28_I2.b; CP: C29_I1.b; PUM-CP: C91_I1.b). XRPD patterns of bulk samples are reported in a), XRPD patterns of binder-concentrated samples are reported in b). The main diffraction peaks of the mineral phases are highlighted. Abbreviations: Ps-gel = phyllosilicate gels, Bt/Ilt/Ms = biotite/illite/muscovite; AFm = AFm phases; Chl = clinochlore; Anl = analcime; Qz = quartz; Vtr = vaterite; Or = orthoclase; Sa = sanidine; Ab = albite; Cal = calcite; Di = diopside; Ap = hydroxyapatite; Hem = hematite; Zin = zincite (internal standard); Hl = halite.

compositional profile given by anthropogenic calcite, finely powdered pozzolanic additives and pozzolanic reaction products, with an additional cryptocrystalline Mg, Al-rich component. Porosity is slightly higher than ASH renders and mainly constituted of irregular vughs with dimensions of several hundred μm.

XRPD-QPA's (Table 2, Fig. 8a) showed variable amounts of calcite and silicate phases, suggesting an inhomogeneity in the relative lime/aggregate proportions, while the paracrystalline phase related to the pozzolanic additives and the reaction products is always high. Furthermore, all the analyzed renders are characterized by the occurrence of clearly detectable amounts of structurally disordered phyllosilicate gels. They are present within the renders in amounts from 2.4 wt% to 5.7 wt%, directly correlated with the Mg and Al enrichments in the binding matrices. This evidence indicates they are disordered Mg-rich phyllosilicates whose occurrence in Roman mortars was already observed [32].

c) *Cocciopesto renders (CP)*. These renders are always found in coating systems corresponding to re-plastering phases, except for C29, constituted only of this class of binding materials, and C91, where it constitutes the base layer. Furthermore, its application is attested in the Roman well of C92 cistern. In any case, CP ren-

ders are never placed below ASH and ASH-CP ones. They are applied both as centimetric base layers and millimetric finishing layers. Macroscopically, they are characterized by medium to high cohesion and colors ranging from white (5YR-8/1) to pinkish (5YR-8/2) (Fig. 3c). B/A ratios are highly variable, and the aggregate fraction is characterized by a bimodal distribution, moderately sorted (Fig. 4e, f).

Coarser aggregate particles are constituted of dominant angular crushed ceramics fragments, with 5 mm maximum size in the base layers and finer than 2 mm in the finishing ones, discriminable in two main types. The first one (Fig. 6a) is characterized by pale pinkish colors (5YR-8/3) and is constituted of partially vitrified siliceous-aluminous matrices, high in Ca (Fig. 6c1), with a temper fraction constituted of an association of silicate phases affine to the natural sand aggregate within the renders and carbonate foraminifera bioclasts, whose permanence indicate the adoption of firing temperatures below the typical carbonate calcination thresholds [33]. Interfacial pozzolanic reaction rims are almost totally absent. The second one (Fig. 6b) is a highly vitrified, low calcic crushed ceramics fraction (Fig. 6c2) affine to the one observed in ASH-CP renders, with clear interfacial pozzolanic reaction rims. The finer aggregate fraction is constituted of ceramics powder, associated to quartz, sandstone, andesite and carbonate clasts, rare *foraminifera* bioclasts and sporadic feldspars and femic minerals.

The binder matrices are characterized by heterogeneous textures (Fig. 4f), with dense aggregates of microcrystalline anthropogenic calcite recognizable by the typical high interference colors, associated to optically extinct clusters of cryptocrystalline phases, suggesting the occurrence of finely powdered ceramics and paracrystalline hydrated phases due to pozzolanic reaction processes between the glassy component of the ceramic powder and the lime binder [34,35]. The backscattered electrons imaging of the binder matrices showed a remarkable mean atomic number variability, as indicated by the heterogeneity of the backscattered electrons (BSE) signal (Fig. 7e). EDS microanalyses indicated a mainly calcic composition for the areas characterized by lighter BSE signal (Fig. 7f2), confirming the occurrence of anthropogenic carbonates, while the darker areas are characterized by a heterogeneous silico-aluminous-calcic-magnesian composition with minor amounts of alkalis and iron (Fig. 7f1), confirming the occurrence of the pozzolanic additive. The volumetric ratios between anthropogenic calcite and pozzolanic materials are highly variable among samples. Few sub-millimetric lime lumps are generally present, approximately 3–5 vol% over the total matrix (Fig. 7e). The pore network is mainly constituted of diffuse vescicles/vughs (around 20 vol%), likely related to an excess of water in the lime putty, while planar voids and channels are rare.

XRPD analyses (Table 2, Fig. 8a) highlighted strong variations in the relative proportions between calcite, silicate phases and paracrystalline fraction, fully consistent with the observed fluctuations in the amounts of constituting components.

d) *Pumice-cocciopesto renders (PUM-CP)*. These renders are always found in re-plastering coating systems, alone or over ASH-CP and CP renders, both as centimetric base layers and millimetric finishing ones. They are macroscopically characterized by variable cohesive properties, from low to medium-high, and colors varying from pinkish-white (2.5Y-8/2) to pale yellow (2.5Y-7.4) (Fig. 3d). B/A ratios are typical for normal/slightly fat renders, with a moderately sorted aggregate fraction characterized by a unimodal granulometric distribution centered within the medium sands granulometric range. Compositionally, it is constituted by an association of natural sand and rounded pumice clasts in variable proportions, with a secondary fraction represented by angular crushed ceramics fragments (Fig. 4g).

The natural sand fraction is affine to the one observed in the previous classes of renders, while pumice clasts are in form of vesicular hypocrystalline aggregates (Fig. 4h, 6e) with sanidine phenocrysts and a glassy fraction of silico-aluminous-potassic composition with traces of sodium, calcium and iron (Fig. 6f2), showing diffuse interfacial dissolution features related to pozzolanic reaction processes. Crushed ceramics fragments (Fig. 6d) are highly calcic (Fig. 6f1), with several un-calcined bioclast residues and almost devoid of pozzolanic reaction rims, as observed in the first class of ceramic particles of CP renders.

The binding matrices are mainly constituted by dense optically extinct clusters of cryptocrystalline phases (Fig. 4g, 7g), with a chemical composition compatible both with the glassy fraction of pumice clasts and the partially vitrified ceramic matrices, except for significant enrichments in calcium, which is often the dominant chemical element (Fig. 7h1, h2). Such evidence indicates a compositional profile given by anthropogenic calcite, finely powdered pozzolanic additives and, possibly, pozzolanic reaction products. Clusters of almost pure anthropogenic calcite are also present in the matrices, both as micrometer-sized lumps and millimeter-sized areas of carbonated matrix. Porosity is highly variable (from 5 to 30 vol%), with prevalent vughs/vescicles likely related to an excess of water in the slaked putty.

XRPD analyses (Table 2, Fig. 8a) highlighted fairly homogeneous mineralogical profiles, with abundant fractions of anthropogenic calcite, high amounts of paracrystalline phases related both to the glassy fraction of pumices and crushed ceramics fragments and to possible paracrystalline pozzolanic reaction products, and a heterogeneous silicate fraction related both to the local natural sand and the mineral components of pumice grains (sanidine and analcime).

e) *Lime putty renders (PL)*. These renders have been observed sporadically and they have been used as finishing layers (0.05 up to 2 mm thick), likely to confer a white uniform color to the surface of the coatings. They are mainly constituted of pure carbonated lime, although sporadic aggregate fractions composed of local sand may be present.

f) *Concretes with crushed ceramics (CCC)*. This type of concrete has been observed in all the 4 samples of cistern floor coatings. The binder matrix is characterized by a homogeneous carbonate microcrystalline texture, with a reduced porosity (< 10 vol%), mainly constituted of vughs and vescicles. Aggregates are homogeneously distributed and sorted, with a planar orientation which suggests an intentional mechanical compaction of the binding mixture. They present a bimodal granulometric distribution due to their bi-component nature. The main constituents are angular centimeter-sized crushed ceramics fragments (Fig. 3e, 4i, 4j), highly vitrified and oxidized, with a minor occurrence of rounded sandstone and andesite gravel aggregates of local origin [25]. Furthermore, a fine aggregate fraction is present, compositionally and texturally similar to the local sand component of the previous classes of renders. Despite the potential pozzolanicity of the ceramic aggregates, their low specific surface and the absence of finely ground ceramics powder generally limits hydraulic reactions to reduced interfacial portions [34–36], as already observed for this class of Roman concretes employed as floor beddings or revetments [31].

Table 3
Composition of the selected binder-concentrated samples of the render mixes employed in the Nora cisterns, obtained by a combination of full profile fitting of the experimental XRPD patterns according to the Rietveld method, acid treatments for the discrimination of the paracrystalline fractions, and TOC measurements for the determination of the fraction of organic carbon.

Sample	Type	Composition (wt.%)													
		Calcite	Vaterite	Mg-AFm	Ca-AFm	Quartz	Diopside	Hematite	Illite/Muscovite	Ps-Gel	Hydroxyapatite	Halite	Organic Carbon	Soluble Amorphous	Insoluble Amorphous
C13_I1.a	ASH	38.7	1.5	6.7	0.0	0.3	0.0	0.0	1.3	0.0	0.6	0.0	1.3	20.5	29.1
C28_I2.b	ASH-CP	24.8	0.0	1.6	0.5	0.4	2.2	0.2	0.8	17.0	1.3	0.0	2.1	36.3	12.8
C29_I1.b	CP	29.1	0.0	0.0	1.3	0.6	0.0	0.1	1.6	0.0	0.0	1.3	0.0	40.5	25.6
C91_I1.b	PUM-CP	17.4	0.0	0.0	0.0	0.6	0.0	0.0	1.7	0.0	0.0	0.0	0.0	38.9	41.4

Table 4
Total Organic Carbon (TOC) and stable isotopic composition of carbon ($\delta^{13}C$) of selected binder-concentrated samples of the render mixes employed in the Nora cisterns.

Sample	Type	TOC (wt.%)	δ13C (‰)
C2_I1.b	ASH-CP	2.0	−24.5
C13_I1.a	ASH	1.3	−23.3
C28_I2.b	ASH-CP	2.1	−24.9
C92_I2.a	ASH-CP	2.1	−23.8

4.3. Mineralogical and spectroscopic characterization of the binder fractions

4.3.1. Composition of the binder fractions

The compositional profile of the ASH binder-concentrated sample (Table 3, Fig. 8b) presents anthropogenic calcium carbonates as main component, followed by the insoluble paracrystalline fraction, identifiable as the non-reacted ash fraction, and the soluble paracrystalline fraction, ascribable to the paracrystalline component of the pozzolanic reaction products (C-S-H and AFm phases), prone to dissolution under acidic conditions [37,38]. Furthermore, relevant amounts of poorly crystalline carbonate-AFm phase were detected, whose best fit was obtained with a Mg-based hydrotalcite structure. Reduced amounts (<2 wt%) of silicate phases are present, related to contaminations of the finer aggregate fractions. Furthermore, the occurrence of reduced but clearly detectable aliquots of hydroxylapatite confirms the partial animal origin of the combustion residues, which are characterized by a fraction of organic carbon of 1.3 wt% with an isotopic composition of −23.3‰ VPDB (Table 4). The value is somehow heavier than the average isotopic composition of C3 plants in non-desert Mediterranean environments (ca. −26.5‰ VPDB, according to Ref. [39]). This could be explained by the incorporation of organic matter from either C4 plants or animals in the render recipe. The latter is supported by the occurrence of hydroxyapatite in the binder-concentrated sample and by the observation of bone fragments through microscopic techniques.

The ASH-CP binder-concentrated sample (Table 3, Fig. 8b) is mainly composed of soluble paracrystalline phases likely related to the pozzolanic reaction products, followed by anthropogenic carbonates and insoluble paracrystalline compounds ascribable to the unreacted pozzolanic products (ceramics powder and ash). Furthermore, significant aliquots of phyllosilicate gels have been detected, which resulted insoluble in the acidic solution. The diffraction contributions of these compounds are limited to few broad maxima of low diffracted intensity, some of them markedly asymmetric, typical for lamellar and turbostratic structures with nanometer-sized coherent scattering domains. Furthermore, their angular positions and profile characteristics present marked similarities with the ones of magnesium-silicate-hydrate (M-S-H) gels formed in modern high Mg Portland-based blend cements such as blast furnace slag cements [40,41], or after interaction between Portland-based binders and clay minerals [42–44]. Such phases have been described as poorly crystalline 2:1 talc-like structures [41,45]. The slight discrepancies between the experimental and literature data, such as the translation toward lower angular values of the first reflection corresponding to the layer-to-layer basal distance, may be attributed to the incorporation of Al within the crystal structure, suggesting the occurrence of a M-A-S-H gel with a saponite-like structure. This is in accordance with the observed Mg and Al enrichments in the binder matrices of the ASH-CP renders. Apart from the main components, reduced aliquots of poorly crystalline carbonate-AFm phases were detected, both Mg- (hydrotalcite) and Ca-based (hydrocalumite). Furthermore, the hydroxylapatite occurrence confirms the partial animal origin of the combustion residues also for this class of renders. The higher amounts of the phase with respect to the ASH sample indicate that finer fractions of combustion residues were added in greater extents to the original mixes, as confirmed by the higher organic carbon aliquots, always above 2 wt% (Table 4). The isotopic composition of organic carbon in the analyzed samples is between −24.9 and −23.8‰ VPDB (Table 4). As observed for the ASH sample, the heavier values with respect to the average isotopic composition of C3 plants in non-desert Mediterranean environments support the incorporation of animal-related organic matter in the render mixes. Finally, scarce aliquots of silicate and oxide phases are present. They are related to the residual fine aggregate fractions, apart from diopside and hematite, likely identifiable as high-temperature firing products of the ceramic powder additive [33].

The analyzed CP binder-concentrated sample (Table 3, Fig. 8b) is mainly constituted of anthropogenic calcite and paracrystalline phases, the latter is more than double the former. The insoluble unreacted residue of ceramic powder is lower than the soluble paracrystalline pozzolanic phases, and a reduced aliquot of poorly crystalline Ca- based carbonate-AFm phase was detected. Aggregate and firing-derived crystalline phases are present in concentrations around 2 wt%, and reduced halite aliquots were detected, likely correlated to marine salts depositions [46].

Finally, an association of anthropogenic calcite and paracrystalline phases constitutes the PUM-CP binder-concentrated sample (Table 3, Fig. 8b), with the latter significantly higher than the former and characterized by a slight prevalence of insoluble residues of pozzolanic additives over soluble paracrystalline pozzolanic phases. Residual silicates are present in concentrations around 2 wt%.

4.3.2. Spectroscopic characterization of the binder fractions

The analysis of the ^{29}Si and ^{27}Al MAS-SS-NMR spectra obtained from the binder-concentrated fractions provided better insights on the incidence of pozzolanic reaction amongst the determined classes of renders. More in detail, the analysis of the −60 – −120 ppm ^{29}Si chemical shift is crucial for the determination of the degree of condensation of SiO_4 tetrahedra [47], while the analysis of the 90 – −40 ppm ^{27}Al chemical shift region gives information on the coordination of Al atoms [48].

Nevertheless, the discrimination of siloxane units according to the number of covalent bonds in the polymer network bonded over a bridging oxygen is perturbed in the analyzed systems by the aluminosilicate nature of the employed pozzolanic additives and, most likely, of the silicate-based pozzolanic products (M-A-S-H and C-A-S-H phases [49]). Indeed, the replacement of silicon atoms by aluminum in the second coordination sphere significantly influences the resulting chemical shift in the obtained ^{29}Si MAS NMR spectra [47]. Furthermore, as a consequence of the paracrystalline nature of the analyzed constituents (pozzolanic additives and pozzolanic phases), the corresponding ^{29}Si NMR signals of the individual units are usually broadened, overlapping each other, thus creating a large broad signal without characteristic features (Fig. 9a) [47]. In this perspective, a detailed deconvolution of the resulting ^{29}Si MAS NMR spectra was discarded in favor of a more qualitative interpretation of the extent of the pozzolanic reaction by considering the shift of the fitted center of the peak from very negative chemical shift values (completely condensed Q^4 siloxane building units of the unreacted pozzolanic additives [45] at about −100/−105 ppm) to less negative chemical shift values (Q^1 and Q^2 siloxane dimers and chains of the C-S-H/C-A-S-H phases [50] at about −85 ppm). According to this analytical interpretation (Table 5, Fig. 9a), ASH renders are the ones showing the lower extent of silicates pozzolanic reaction (maximum of distribution at −101 ppm), while a progressive increase in the reaction rate is observed in PUM-CP renders (maximum of distribution at −97.1 ppm), CP renders (maximum of distribution

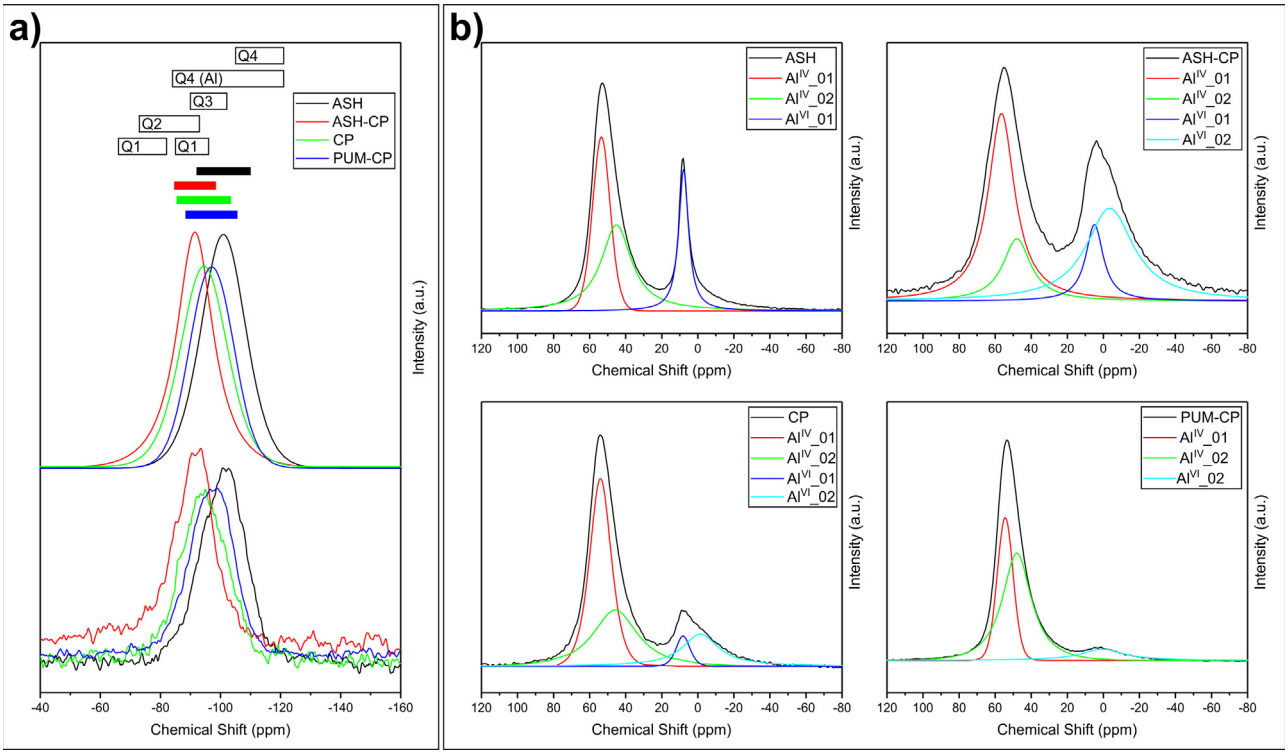

Fig. 9. a) ^{29}Si MAS-SSNMR analyses of representative binder-concentrated samples for each render typology applied in the Nora cisterns (ASH: C13_I1.a; ASH-CP: C28_I2.b; CP: C29_I1.b; PUM-CP: C91_I1.b). The raw spectra are reported below, while the fitted peaks are reported above, together with the FWHM bars and the typical intervals for Q^1, Q^2, Q^3 and Q^4 SiO_4 tetrahedra [41,42]. b) ^{27}Al MAS-SSNMR spectra of representative binder-concentrated samples for each render typology applied in the Nora cisterns (ASH: C13_I1.a; ASH-CP: C28_I2.b; CP: C29_I1.b; PUM-CP: C91_I1.b), reporting the fitted peaks.

Table 5
Results of the fitting procedure on the ^{29}Si MAS-SSNMR spectra of the binder-concentrated samples of the render mixes employed in the Nora cisterns. Center of the fitted peaks and their full widths at half maximum (FWHM) are reported.

Sample	Type	Center (ppm)	FWHM (ppm)
C13_I1.a	ASH	−101.0	17.5
C28_I2.b	ASH-CP	−91.5	14.2
C29_I1.b	CP	−94.5	18.2
C91_I1.b	PUM-CP	−97.1	17.3

at −94.5 ppm) and ASH-CP renders (maximum of distribution at −91.5 ppm). These data are in line with the determined ratios of soluble over insoluble paracrystalline phases in the analyzed samples. Furthermore, despite the high concentrations of phyllosilicate-based M-S-H phases in the ASH-CP sample, which would imply an increase in the relative NMR contributions within the chemical shift ranges of Q^3 siloxane building units, the overall signal of the sample is mainly shifted toward the typical regions of Q^1 and Q^2 sites. This is in accordance with the small size of the phases in the *ab* plane due to their nanocrystalline characteristics, implying relevant truncation of the silica sheets with consequent increase of edge sites density [45].

The ^{27}Al MAS-SS-NMR spectra of the analyzed samples are always characterized by the presence of two distinct peaks (Fig. 9b). The main one is an asymmetric peak with maximums of distribution within typical chemical shift intervals of tetra-coordinated $^{IV}[Al^{+3}]$ atoms in chemical environments characterized by the occurrence of Q^4 siloxane units in the second coordination sphere [48]. This region of the spectrum (−60 to −40 ppm) has been fitted in all the analyzed samples with two peaks, a narrower one with maximums of distribution between 53.5 and 56.5 ppm, and a wider one with maximums of distribution between 45.2 and 48.0 ppm (Table 6, Fig. 9b). Both peaks may be ascribed to the Al atoms in the distorted tetrahedral networks of both the paracrystalline silica-based pozzolanic phases, corroborating the hypothesis of C-A-S-H and M-A-S-H gels formation, and the unreacted residues of the amorphous pozzolanic additives. Interpreting the relative intensities of the two peaks in light of the reactivity deduced by XRPD analyses, the peak at higher ppm values may be ascribed to the pozzolanic phases, showing higher intensity in the most reacted CP and ASH-CP samples. On the other hand, the one at lower ppm values, more intense in the less reacted ASH and PUM-CP samples, may be associated to the NMR contribution related to the unreacted pozzolanic additives.

Furthermore, all the spectra are characterized by the occurrence of a secondary isolated peak with maximums of distribution within typical chemical shift intervals of Al atoms in hexagonal Al^{VI} coordination (in the region approximately −20 to 0 ppm) [48] (Fig. 9b). The peak presents symmetric shape and maximum of distribution at 7.9 ppm in the analyzed ASH sample, and it is likely related to the Al atoms in the octahedral sites of Mg-based carbonate AFm phase [51], whose abundant occurrence was already determined by XRPD. In the ASH-CP samples, the peak is asymmetric and it has been fitted by the convolution of two peaks (Table 6, Fig. 9b), a narrower one with maximum of distribution at 4.9 ppm and likely related to the Al atoms in the octahedral sites of carbonate AFm phases, and a main wider one with maximum of distribution at −3.6 ppm. This peak is to be ascribed to the Al atoms in the octahedral sites of M-A-S-H phases, suggesting a partial dioctahedral nature of the anthropogenic phyllosilicate gels. The analyzed CP sample is as well characterized by an asymmetric secondary peak, fitted with a first sub-peak centered at 8.2 ppm and likely ascribable to the Al atoms in the octahedral sites of Ca-based carbonate AFm phase, and a main wider one centered at −1.5 ppm (Table 6, Fig. 9b). This second contribution may be related to the Al atoms in the distorted octahedral sheets of partially calcined clays of the crushed ceramics fraction

Table 6
Results of the fitting procedure on the ^{27}Al MAS-SSNMR spectra of the binder-concentrated samples of the render mixes employed in the Nora cisterns. Peak types, relative area fractions, centers of the fitted peaks and their full widths at half maximum (FWHM) are reported.

Sample	Type	Peak type	Area Fraction (%)	Center (ppm)	FWHM (ppm)
C13_I1.a	ASH	Al^{IV}_01	32.3	53.5	11.6
		Al^{IV}_02	45.6	45.2	20.2
		Al^{VI}_01	22.1	7.9	6.4
C28_I2.b	ASH-CP	Al^{IV}_01	39.9	56.5	17.8
		Al^{IV}_02	13.9	48.0	18.7
		Al^{VI}_01	10.8	4.9	11.7
		Al^{VI}_02	35.4	−3.6	32.0
C29_I1.b	CP	Al^{IV}_01	46.1	54.0	14.0
		Al^{IV}_02	31.5	45.8	28.8
		Al^{VI}_01	4.7	8.2	9.0
		Al^{VI}_02	17.7	−1.5	24.2
C91_I1.b	PUM-CP	Al^{IV}_01	34.1	54.4	10.4
		Al^{IV}_02	55.4	48.0	18.8
		Al^{VI}_02	10.4	0.5	28.3

fired at lower temperatures. Such hypothesis is corroborated by the presence of a secondary isolated peak with broad full width at half maximum and centered at comparable ppm values (0.5 ppm) in the PUM-CP sample (Table 6, Fig. 9b), which presents the same crushed ceramics type in the render mixture.

5. Discussion

5.1. Chronology and cultural influences

A crosscheck between render typologies and their articulation in diachronic coating phases distinguished several coating systems, constituted of up to 4 render layers and clustered within 3 main groups (Fig. 10):

a. Coating systems 1 (CS1) are made of 1 or 2 render layers rich in combustion residues and they can be distinguished into two subgroups. In the CS1a system, preparatory and finishing layers are both made of ASH render, as attested in cistern C13, while in CS1b system ASH-CP renders were generally employed. A thin layer of pure lime render (PL) is sometimes set as superficial polishing.
b. Coating systems 2 (CS2) present at least one layer made of PUM-CP render and they are subdivided in two subgroups. The first one (CS2a) is usually composed of 1 or 2 preparatory layers of ASH-CP render, while the finishing one is made of PUM-CP render. In the second variance (CS2b), all layers are made of PUM-CP renders (i.e. later restorations of cisterns C4 and C5), sometimes with a preparatory one made of CP render (i.e. C91).
c. Coating systems 3 (CS3) are rare and are usually composed of 1 up to 3 CP layers, with an increasing comminution of the ceramic aggregate towards the external portions.

Concerning floors, all Nora cisterns present only one layer of concrete with crushed ceramics (CCC). No restorations have been identified, so it is possible to assume that such floors were much more durable than wall renders, which needed several repair interventions.

Analyzing the sequences of the wall coating systems under a stratigraphic and chronological perspective, CS1 systems are always placed in direct contact with masonry (Fig. 10), thus they can be identified as the oldest ones in terms of relative chronology, while CS2 systems are almost exclusively employed for restorations apart from one case (C91). Considering absolute chronologies of properly excavated cisterns, a single parietal coating activity made of a CS1 system may be observed in the cistern excavated in the Roman *forum* (C2), which was made in the second half of 2nd century B.C.E. and obliterated before the building of the *forum* in the second half of 1st century B.C.E. [2]. This chronological constraint matches published radiocarbon analyses on a charcoal fragment taken from the inner ASH-CP render layer of C92 cistern, providing a *terminus post quem* for the conversion of this Punic grave into a cistern between the 2nd century and the first half of the 1st century B.C.E. [4,52]. These two well-dated contexts provide a good chronological constraint for the introduction of CS2 system. In fact, this technique is employed as original coating only in the cistern excavated in the "Favonia house" (C91). This is a housing context established, according to preliminary data, between the 1st and the 2nd century C.E. [53]. However, these well-dated contexts are exceptions when compared with the majority of Nora cisterns, which were excavated without stratigraphic methods in the 1950s. Nevertheless, relative sequences could demonstrate a progressive shift in production technologies from systems employing mainly ASH and ASH-CP renders (CS1a, CS1b) to pumice-based systems (CS2b), with CS2a systems possibly representing a transitional phase.

Comparing the results of this research with other studies performed on cistern wall renders, relevant similarities are observable between the Nora technologies and the ones employed in several Mediterranean sites. Archaeometric analyses indicated the presence of cistern coatings based on ash renders mixed with sporadic crushed ceramics in other sites of Sardinia, such as Tharros [54,55]. Furthermore, similar renders are commonly found in Carthage at least from the 4th century B.C.E. to the late Punic period [46,56,57]. Therefore, this practice might represent a technological specificity of the Punic building tradition, with a recurrent use documented in several Punic centers of the western Mediterranean [58–60]. This use of charcoal and ash particles as pozzolanic additives in mortars and renders was later preserved in Carthage also during Roman and Byzantine times [46], in addition to crushed ceramics. Carthaginians probably knew the pozzolanic properties of *cocciopesto* mortars, most likely derived from the Aegean tradition [61], as house floor coatings are often layered with such material, the so-called *opus signinum* [62,63]. Nevertheless, the use of abundant fractions of crushed ceramics for cistern wall renders appears to be uncommon, apart from rare cases [64]. Considering CS1 systems as the result of a technological transfer in Nora, brought about by Carthaginian craftsmen during the Punic domination of Sardinia and still in use during the Roman Republican period, the production of ASH-CP renders rich in crushed ceramics could be ascribed to a combination of Punic practices with the traditional *cocciopesto* technique, frequently employed by Romans for floor and parietal coatings.

On the other hand, pumice occurrence in renders strongly recalls the *pulvis puteolana* cited by Vitruvius in his treatise *De Architectura* [65] and commonly employed and traded in Roman times at least since the 1st century B.C.E., as attested by the occurrence of

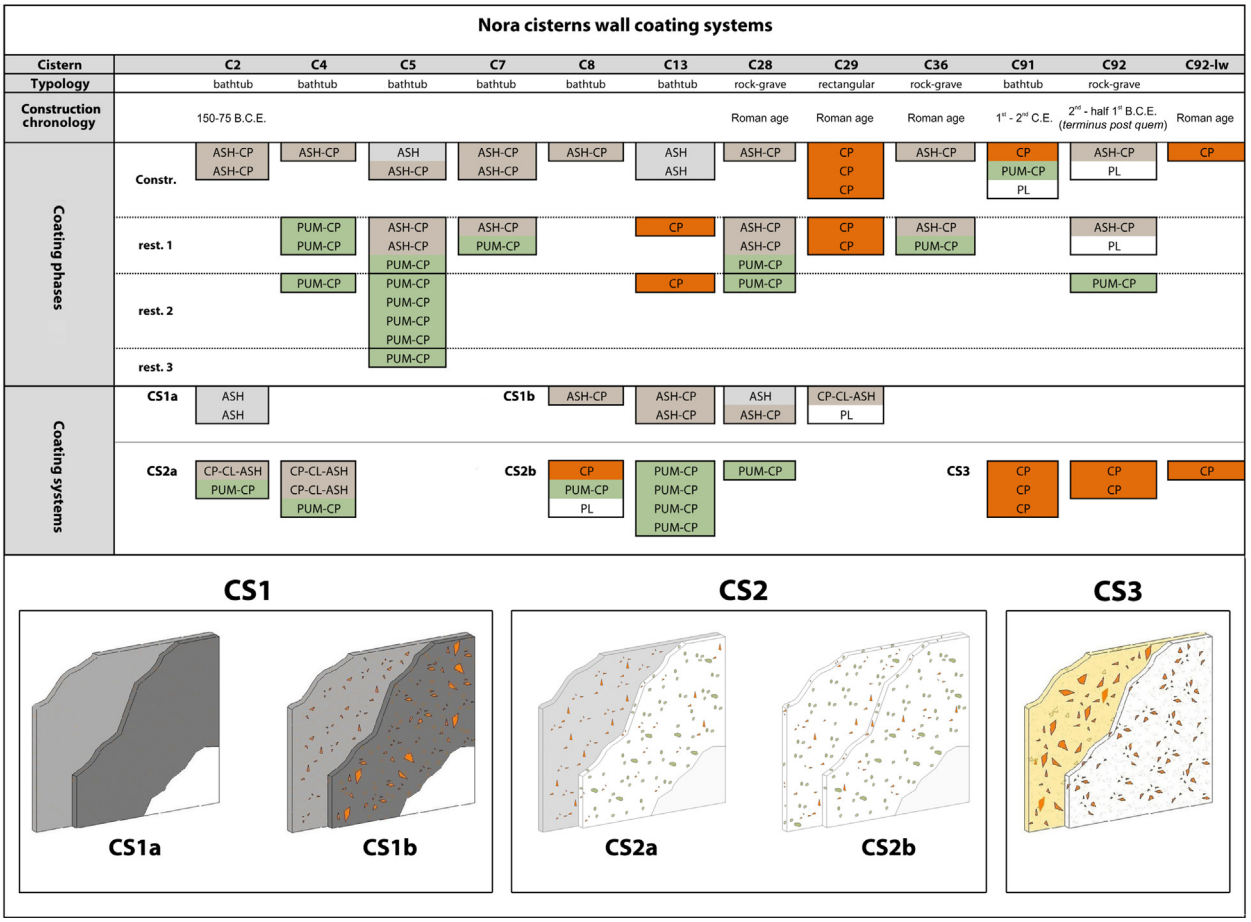

Fig. 10. Coating systems of the Nora cisterns. Render typologies and discrimination of the plastering activities (construction/restorations) are reported in the upper part of the figure. Graphical representations and compositional variances of render strata for each coating system are reported in the bottom of the figure.

Phlegraean pyroclastic sands in the concrete structures of several harbors along the Mediterranean Sea [66]. *Pozzolanas* have been found also in loads of Roman shipwrecks as the ones discovered in Pisa [67,68]. Several pyroclastic deposits were exploited in ancient times, also before the time of Vitruvius, and it has been proven that even Carthaginians knew the pozzolanic properties of tuffs and pumices, again a knowledge likely derived from the Aegean world [56,57,61,69,70]. However, even if the properties of volcanoclastic aggregates appear to be known by Punics, a diffuse utilization of pumices seems to be related to the Roman period, as suggested by the lack of use of CS2 systems in the cisterns of Nora dated before the imperial age. Further geochemical analyses on pumice clasts aimed at identifying their provenance will provide a useful tool to solve this problem.

Lastly, CS3 systems seem to be the most closely related to Roman traditional *cocciopesto*. In fact, also the rectangular shape of the cistern appears unusual in Punic societies.

5.2. Materials technology

Under a technological perspective, the variation of ancient mix designs formulated by Roman craftsmen under diverse cultural influences deeply influenced the cohesion and durability of the coating systems, shifting the reaction of lime-based binding mixtures from standard aerial carbonation.

In ASH renders, the addition of organic matter combustion residues may be interpreted as an intentional technological choice to increase the pozzolanic properties of the binding mixtures, and thus the water-sealing capacity of the cisterns. Inorganic ash residues of animal origin like dung ash, whose at least partial occurrence was demonstrated in the analyzed samples, are constituted of highly amorphous, mainly aluminosilicate compounds [27], thus characterized by potential pozzolanicity. Nevertheless, its addition to ASH renders produced only a partial pozzolanic effect favoring the formation of alumina-based compounds over silica-based ones, whose crystalline features are less efficient for binding purposes [37]. The resulting AFm phases were mainly Mg-based, indicating autogenous reaction of the ash clusters after dissolution in alkaline solution without significant interaction with the calcic component of the lime binder, with a consequent shift toward the aerial reaction in the competition between carbonation and hydration of the pozzolanic system [71]. Such processes may have been influenced by the low specific surface of the pozzolanic additive, whose sandy dimensions indicate an addition within the render mixture without significant comminution processes.

More pronounced pozzolanic properties were observed in the render typologies based on crushed ceramics and pumice, especially the CP ones, characterized by a higher degree of reaction of both the silicate and the aluminate components with respect to the PUM-CP ones. Such different properties may be related both to the lower specific surface of pumice particles with respect to the fine ceramic powder of CP renders, and to the exclusive employment of pozzolanic additives derived from low temperature, less vitrified ceramics in PUM-CP renders.

Nevertheless, the more pronounced pozzolanic properties were observed in ASH-CP class of renders. Despite their proportional inhomogeneity, the simultaneous addition in the binding mixtures of amorphous, aluminosilicate-based combustion ashes and pow-

ders derived from highly vitrified ceramics led to the best overall pozzolanic properties, with the highest reaction degree of silicates and still a remarkable level of hydrous calcium aluminates precipitation. Such marked pozzolanic properties may have been influenced by specific treatments of the pozzolanic additives before and during the render mixing, such as a comminution of the combustion residues, possibly through co-grinding with the ceramic scraps, which led to greater amounts of fines in the mixture and consequent improved pozzolanic reactivity due to the higher specific surface. Furthermore, the systematic occurrence of chlorine and sodium both in the binding matrices and in the pozzolanic lumps may suggest the employment of saltwater during render preparation. It has been demonstrated that salt content in lime-based pozzolanic systems increases silicates dissolution, due to the pH increase promoted by sodium hydroxide formation after the interaction between calcium hydroxide and sodium chloride [72,73], thus the utilization of saltwater in place of freshwater may be considered an intentional choice of Roman craftsmen to enhance renders' binding properties. Finally, a relevant contribution in the final cohesive and water-sealing properties of ASH-CP renders may be ascribed to the formation of M-S-H/M-A-S-H phyllosilicate gels during the pozzolanic reaction processes together with C-S-H/C-A-S-H products. The precipitation of these nanostructured anthropogenic compounds was favored thanks to the shift of the chemical system into the Si/Al/Mg stability fields [45] at high silica and alumina activities [41], which was promoted by the simultaneous employment of Mg-rich pozzolanic additives such as animal ashes [28] and crushed ceramics. Furthermore, apart from their contribution to the overall strength and durability properties of renders, the precipitation of nanostructured phyllosilicates having high specific surface area and marked water absorption and cationic exchange capacities [74,75], should have further beneficiated the long-term operative conditions of the cisterns, both in terms of leakage/infiltration prevention and filtering behavior against chemical pollutants.

6. Conclusions

This paper has investigated the cultural influence of Punic and Roman technological traditions in the Mediterranean area, taking as a benchmark the evolution of the coating systems used to waterproof several cisterns in the ancient city of Nora (Southern Sardinia). The analytical approach applied to characterize the render layers of the systems, based on a combination of mineralogical and spectroscopic techniques, allowed not only a discrimination and categorization according to their compositional profiles functional to the definition of relative and absolute plastering chronologies, but also to decipher the reactive processes responsible for their final cohesive and waterproofing properties.

From a socio-cultural perspective, CS1a system, employing ASH renders based on combustion residues, faithfully recalls Punic traditions, while CS1b systems, widely employing ASH-CP renders based on a combination of combustion residues and broken ceramics, refer to Punic traditions probably influenced by Roman practices. CS2b systems, mainly employing PUM renders based on pumiceous aggregates, seem to be related to Roman traditions, even though late Punic influences cannot be totally excluded, while CS2a systems employing both ASH-CP and PUM renders could represent a transition phase between CS1b and CS2b. Finally, CS3 systems, based on broken ceramics, seem to be fully ascribed to Roman practices.

The obtained results confirm how Punic practices and traditions were still adopted in construction techniques in Nora over 100 years after the establishment of the province of *Sardinia et Corsica*, as observed for building techniques and metric standards [2,76,77]. This shows, once again, how the real technical-cultural Romanization of the island occurred long after the institutional date of 227 B.C.E., with a long series of older influences maintained for decades [78], directly influencing composition and properties of materials.

Indeed, even though Roman renders showed better pozzolanic properties with respect to Punic ones, the best overall characteristics in terms of degree of hydraulic reaction, cohesion and waterproofing capacity were observed in ASH-CP renders, constituting a clear example of technological synthesis conjugating in its complex mix design both Punic and Roman traditions. Such excellent properties were significantly influenced by the precipitation of M-S-H/M-A-S-H phyllosilicate gels, reported for the first time in ancient binders.

The study of magnesium-silicate-hydrates formation in modern cementitious systems has been the subject of a growing interest in recent times, thanks to their potential applications in low pH binding composites for waste encapsulation and refractory systems [79–81] and to their excellent mechanical and durability properties when compared to classic Ca-based cements [82–85]. Their pervasive precipitation in ancient binding systems is a further proof of the high level of technological evolution reached by Punic-Roman craftsmen within the complex framework of the Mediterranean cultural *koine*.

Authors contributions

MS, SD and AA designed research; GA and JB supervised the research project; MS, SD and AA performed the samplings; MS, SD, AA and GR performed the samples preparation; MS, SD, AA, ST, NP and GR analyzed the samples; MS, SD, AA, ST, NP and GR performed the data processing and interpretation; SD and JB performed the archaeological analysis; MS drafted Sections 3.2, 4.2, 4.3, 5.2 and 6; SD drafted Sections 2, 3.1, 4.1, 4.2, 5.1 and 6; JB drafted Sections 1 and 6; all authors contributed to the revision of the manuscript.

Acknowledgements

The authors would like to thank the "Soprintendenza Archeologia, Belle Arti e Paesaggio per la città metropolitana di Cagliari e le province di Oristano e Sud Sardegna". The project was carried out in the frame of the Strategic action "Multidisciplinary methodological approaches to the knowledge, conservation and valorization of the cultural heritage: application to archaeological sites" (project: STPD11B3LB_002) supported by University of Padova. Francesca Andolfo is gratefully acknowledged for revising the English text.

References

[1] J. Bonetto, G. Bejor, S.F. Bondì, B.M. Giannattasio, M. Giuman, C. Tronchetti (Eds.), Nora. Sardegna archeologica. Guide e Itinerari, 1, Carlo Delfino Editore, Sassari, 2018.
[2] J. Bonetto, L'insediamento di età fenicia, punica e romana repubblicana nell'area del foro di Nora, in: J. Bonetto, A.R. Ghiotto, M. Novello (Eds.), Nora. Il foro romano. Storia di un'area urbana dall'età fenicia alla tarda Antichità, I. Lo scavo, Edizioni Quasar, Padova, 2009, pp. 41–243.
[3] J. Bonetto, Nora nel V secolo: dall'emporio fenicio alla colonia cartaginese, in: M. Botto, P. Van Dommelen, A. Roppa (Eds.), La Sardegna e il Mediterraneo occidentale nel V sec. a.C., BABesch supplement series, Leuven, in press.
[4] J. Bonetto, C. Andreatta, S. Berto, L. Bison, E. Bridi, M. Covolan, S. Dilaria, A. Mazzariol, M. Ranzato, La necropoli fenicio-punica e le infrastrutture romane nell'area della ex Base della Marina militare, Quaderni Norensi 6 (2017) 169–188.
[5] J. Bonetto, A. Mazzariol, Nuovi dati d'archivio e nuove evidenze archeologiche sulla necropoli punica orientale di Nora (Cagliari), Fold&R 2017-390 (2017) 1–16.
[6] J. Bonetto, Padova a Nora. Didattica, ricerca, innovazione e divulgazione per la storia della città antica, in: J. Bonetto, G. Falezza (Eds.), Vent'anni Di Scavi a Nora. 1990-2009, Edizioni Quasar, Padova, 2011, pp. 43–55.
[7] S. Cespa, Nora. I sistemi di approvvigionamento idrico, Scavi di Nora, VII, Edizioni Quasar, Roma, 2018.

[8] J. Bonetto, S. Cespa, R.V. Erdas, Approvvigionamento idrico a Nora: nuovi dati sulle cisterne, in: M.B. Cocco, A. Gavini, A. Ibba (Eds.), L'Africa romana, XIX, 3, Conference Proceedings (Sassari 16-19 Dicembre 2010), Carocci editore, Roma, 2012, pp. 2591–2624.
[9] F.M. Crasta, C.A. Fassò, F. Patta, G. Putzu, Carthaginian-Roman cisterns in sardinia, in: F.N. Fujimura (Ed.), Proceedings of the International Conference on Rain Water Cistern Systems, University of Hawaii at Manoa, Water Resources Research Center, Honolulu, 1982, pp. 37–45.
[10] A. Mezzolani Andreose, Le cisterne nella Sardegna di età punica: un quadro tipologico e comparativo, in: T. Schäfer, F. Schön, A. Gerdes, J. Heinrichs (Eds.), Antike Und Moderne Wasserspeicherung, Internationaler Workshop (Pantelleria, 11-14 May 2011), VML Verlag Marie Leidorf, Rahden, 2014, pp. 135–155.
[11] A. Munsell, Soil colour chart, GretagMacbeth, New Windsor, 2000.
[12] N. Marinoni, A. Pavese, M. Foi, L. Trombino, Characterisation of mortar morphology in thin sections by digital image processing, Cem. Concr. Res. 35 (2005) 1613–1619.
[13] H. Rietveld, A profile refinement method for nuclear and magnetic structures, J. Appl. Crystallogr. 2 (1969) 65–71.
[14] T. Taut, R. Kleeberg, J. Bergmann, The new Seifert Rietveld program BGMN and its application to quantitative phase analysis, Mater. Struct. 5 (1) (1998) 55–64.
[15] N. Döbelin, R. Kleeberg, Profex: a graphical user interface for the Rietveld refinement program BGMN, J. Appl. Crystallogr. 48 (2015) 1573–1580.
[16] W. Dollase, Correction of intensities for preferred orientation in powder diffractometry: application of the March model, J. Appl. Crystallogr. 19 (1986) 267–272.
[17] G.W. Brindley, Order-disorder in clay mineral structures, in: G.W. Brindley, D. Brown (Eds.), Crystal Structures of Clay Minerals and Their X-Ray Identification, Mineralogical Society, London, 1980, pp. 125–196.
[18] K. Ufer, G. Roth, R. Kleeberg, H. Stanjek, R. Dohrmann, J. Bergmann, Description of X-ray powder pattern of turbostratically disordered layer structures with a rietveld compatible approach, Zeitschrift für Kristallographie 219 (2004) 519–527.
[19] S.I. Tsipursky, V.A. Drits, The distribution of octahedral cations in the 2:1 layers of dioctahedral smectites studied by oblique-texture electron diffraction, Clay Miner. 19 (1984) 177–193.
[20] A. Addis, M. Secco, F. Marzaioli, G. Artioli, A. Chavarria Arnau, I. Passariello, F. Terrasi, G.P. Brogiolo, Selecting the most reliable ^{14}C dating material inside mortars: the origin of the Padua cathedral, Radiocarbon 61 (2) (2019) 375–393.
[21] L.J. Poppe, V.F. Paskevich, J.C. Hathaway, D.S. Blackwood, A Laboratory Manual for X-Ray Powder Diffraction, U.S. Geological Survey, Coastal and Marine Geology Program, Woods Hole, 2019.
[22] D. Massiot, F. Fayon, M. Capron, I. King, S. Le Calvé, B. Alonso, J.O. Durand, B. Bujoli, Z. Gan, G. Hoats, Modelling one- and two-dimensional solid-state NMR spectra, Magn. Reson. Chem. 40 (2002) 70–76.
[23] R. Ginouvès, R. Martin, Dictionnaire méthodique de l'architecture Grecque et Romaine, Tome I, Matériaux, techniques de construction, techniques et formes du décor, Publications de l'École française de Rome, Rome, 1985.
[24] J.E. Prentice, Geology of Construction Materials, Chapman & Hall, London, 1990.
[25] C.K. Wentworth, A scale of grade and class terms for clastic sediments, J. Geol. 30 (5) (1922) 377–392.
[26] M. Taricco, S. Catalisano, Carta Geologica d'Italia alla scala 1:100000, foglio 240 Ş. Efisio, Istituto Geografico Militare, Roma, 1937.
[27] F. Massazza, Properties and applications of natural pozzolanas, in: J. Bensted, P. Barnes (Eds.), Structure and Performance of Cements, Spon Press, London, 2002, pp. 326–352.
[28] A. Avinash, A. Murugesan, Chemometric analysis of cow dung ash as an adsorbent for purifying biodiesel from waste cooking oil, Sci. Rep. 7 (9526) (2017).
[29] J.S. Pozo-Antonio, Evolution of mechanical properties and drying shrinkage in lime-based and lime cement-based mortars with pure limestone aggregate, Constr. Build. Mater. 77 (2015) 472–478.
[30] T. Matschei, B. Lothenbach, F.P. Glasser, The AFm phase in Portland cement, Cem. Concr. Res. 37 (2007) 118–130.
[31] M. Secco, S. Dilaria, A. Addis, J. Bonetto, G. Artioli, M. Salvadori, The evolution of the vitruvian recipes over 500 years of floor-making techniques: the case studies of the Domus delle Bestie Ferite and the Domus di Tito Macro (Aquileia, Italy), Archaeometry 60 (2) (2018) 185–206.
[32] M. Secco, L. Valentini, A. Addis, Ancient and modern binders: naturally nanostructured materials, in: G. Lazzara, R. Fakhrullin (Eds.), Nanotechnologies and Nanomaterials for Diagnostic, Conservation and Restoration of Cultural Heritage, Elsevier, Amsterdam, 2019, pp. 205–237.
[33] L. Maritan, C. Mazzoli, L. Nodari, U. Russo, Second Iron Age grey pottery from Este (northeastern Italy): study of provenance and technology, Appl. Clay Sci. 29 (2005) 31–44.
[34] G. Baronio, L. Binda, Study of the pozzolanicity of some bricks and clays, Constr. Build. Mater. 11 (1) (1997) 41–46.
[35] J.M. Teutonico, G. Ashall, E. Garrod, T. Yates, A comparative study of hydraulic lime-based mortars, in: P. Bartos, C. Groot, J.J. Hughes (Eds.), Historic Mortars: Characteristics and Tests, Proceedings of the International RILEM Workshop (12-14 May 1999), Paisley, 2000, pp. 339–349.
[36] G. Baronio, L. Binda, N. Lombardini, The role of brick pebbles and dust in conglomerates based on hydrated lime and crushed bricks, Constr. Build. Mater. 11 (1) (1997) 33–40.
[37] H.F.W. Taylor, Cement Chemistry, Thomas Telford Publishing, New York, 1997.
[38] V. Zivica, A. Bajza, Acidic attack of cement based materials a review. Part 1. Principle of acidic attack, Constr. Build. Mater. 15 (2001) 331–340.
[39] A.F. Diefendorf, K.E. Mueller, S.L. Wing, P.L. Koch, K.H. Freeman, Global patterns in leaf 13 C discrimination and implications for the studies of past and future climate, Proc. Natl. Acad. Sci. 107 (2010) 5738–5743.
[40] D.R.M. Brew, F.P. Glasser, The magnesia-silica gels phase in slag cements: alkali (K, Cs) sorption potentials of synthetic gels, Cem. Concr. Res. 35 (1) (2005) 77–83.
[41] D.R.M. Brew, F.P. Glasser, Synthesis and characterization of magnesium silicate hydrate gels, Cem. Concr. Res. 35 (1) (2005) 85–98.
[42] S. Ramírez, J. Cuevas, R. Vigil, S. Leguey, Hydrothermal alteration of "La Serrata" bentonite (Almeria, Spain) by alkaline solutions, Appl. Clay Sci. 21 (2002) 257–269.
[43] A. Dauzères, P. Le Bescop, P. Sardini, C. Cau Dit Coumes, Physico-chemical investigation of clayey/cement-based materials interaction in the context of geological waste disposal: experimental approach and results, Cem. Concr. Res. 40 (2010) 1327–1340.
[44] A. Dauzères, P. Le Bescop, C. Cau-Dit-Coumes, F. Brunet, X. Bourbon, J. Timonen, M. Voutilainen, L. Chomat, P. Sardini, On the physico-chemical evolution of low-pH and CEM I cement pastes interacting with Callovo–Oxfordian pore water under its in situ CO_2 partial pressure, Cem. Concr. Res. (58) (2014) 76–88.
[45] C. Roosz, S. Grangeon, P. Blanc, V. Montouillout, B. Lothenbach, P. Henocq, E. Giffaut, P. Vieillard, S. Gaboreau, Crystal structure of magnesium silicate hydrates (MSH): the relation with 2:1 Mg–Si phyllosilicates, Cem. Concr. Res. 73 (2015) 228–237.
[46] E. Koser, C. Flügel, E. Liebig, E. Karotke, E. Althaus, Punische und kaiserzeitliche mörtel aus dem antiken karthago Erhalten Historisch Bedeutsamer Bauwerke, 1997/1998, 1997, pp. 121–134.
[47] K.J.D. MacKenzie, M.E. Smith, Multinuclear Solid-State NMR of Inorganic Materials, Pergamon, Oxford, 2002.
[48] J. Brus, S. Abbrent, L. Kobera, M. Urbanova, P. Cuba, Advances in ^{27}Al MAS NMR studies of geopolymers, in: G.A. Webb (Ed.), Annual Reports in NMR Spectroscopy, 88, Elsevier, Amsterdam, 2016, pp. 79–146.
[49] M.D. Jackson, S.R. Chae, S.R. Mulcahy, C. Meral, R. Taylor, P. Li, A.H. Emwas, J. Moon, S. Yoon, G. Vola, H.R. Wenk, P.J.M. Monteiro, Unlocking the secrets of Al-tobermorite in Roman seawater concrete, Am. Mineral. 98 (10) (2013) 1669–1687.
[50] P. Colomber, A.R. Grimmer, H. Zanni, P. Sozzani, Nuclear Magnetic Resonance Spectroscopy of Cement-Based Materials, Springer, Berlin, 1998.
[51] G. Artioli, M. Secco, A. Addis, M. Bellotto, Role of hydrotalcite-type layered double hydroxides in delayed pozzolanic reactions and their bearing on mortar dating, in: H. Pöllmann (Ed.), Cementitious Materials: Composition, Properties, Application, Walter De Gruyter GmbH, Berlin, 2017, pp. 147–158.
[52] S. Berto, S. Dilaria, Tomba 3, un approccio multidisciplinare per lo studio dell'ipogeo, Quaderni Norensi 7 (2018) 141–147.
[53] A.R. Ghiotto, G. Fioratto, F.S. Mosimann, A. Zara, L'edificio a est del foro (saggio PO). Campagne di scavo 2014-2015, Quaderni Norensi 6 (2017) 135–142.
[54] C. Del Vais, P. Mattazzi, A. Mezzolani, Saggio di scavo nei quadrati B2.7-8, C2.7-8: la cisterna ad ovest del Cardo, Rivista di Studi Fenici, suppl. 23 (1995) 133–139.
[55] G. Bultrini, A. Mezzolani, A. Morigi, Approvvigionamento idrico a Tharros. Le cisterne, Rivista di Studi Fenici 24 (1996) 103–127.
[56] L.H. Davis, A note on some cistern mortars found at Carthage, in: J.H. Humphrey (Ed.), Excavations at Carthage 1977 Conducted by the University of Michigan, American Schools of Oriental Research, VI, University of Michigan Press, Ann Arbor, 1981, pp. 43–49.
[57] H.G. Niemeyer, R.F. Docter, K. Schmidt, B. Bechtold, Karthago: die Ergebnisse der Hamburger Grabung unter dem Decumanus Maximus, Von Zabern, Mainz, 2007.
[58] M.H. Fantar, Le problème de l'eau potable dans le monde phénicien et punique: les cisternes, Cah. Tunis. 23 (89–90) (1975) 9–18.
[59] A. Prados Martínez, Introduccion al estudio de la Arquitectura pùnica, Ediciones de la Universidad Autónoma de Madrid, Madrid, 2003.
[60] L. Lancaster, Ash mortar and vaulting tubes: agricultural production and the building industry in North Africa, in: S. Camporeale, H. Dessales, A. Pizzo (Eds.), Arqueología de la construcción III. Los procesos constructivos en el mundo romano: la economía de las obras, École Normale Supérieure (Paris, 10-11 Diciembre 2009), Consejo Superior de Investigaciones Científicas, Madrid-Mérida, 2012, pp. 145–160.
[61] G. Artioli, M. Secco, A. Addis, The vitruvian legacy: mortars and binders before and after the Roman world, in: G. Artioli, R. Oberti (Eds.), The Contribution of Mineralogy to Cultural Heritage, European Mineralogical Union, Jena, 2019, pp. 151–202.
[62] V. Vassal, Les pavements d'opus signinum, in: Technique, décor, function architecturale, Archeopress, Oxford, 2006.
[63] Dunbabin K.M.D., The pavements fragments and their typology, In: J. H. Humphrey (Ed.)., Excavations at Carthage 1976 conducted by the University of Michigan, American Schools of Oriental Research, Ann Arbor, 1978, pp. 169-180, (n.d.).
[64] M.H. Fantar, Le temple de Ras ed-Drek, in: F. Barreca, M.H. Fantar (Eds.), Prospezione Archeologica Al Capo Bon II, Consiglio Nazionale delle Ricerche, Roma, 1983, pp. 41–63.
[65] Vitruvius, in: P. Gros, A. Corso, E. Romano (Eds.), De architectura, trans, Giulio Einaudi Editore, Torino, 1997.
[66] Building for eternity, in: C.J. Brandon, R.L. Hohlfelder, M.D. Jackson, J.P. Oleson (Eds.), The History and Technology of Roman Concrete Engineering in the Sea, Oxbow Books, Oxford, 2014.

[67] E. Pecchioni, E. Cantisani, P. Pallecchi, F. Fratini, A. Buccianti, E. Pandeli, S. Rescic, S. Conticelli, Characterization of the amphorae, stone ballast and stowage materials of the ships from the archaeological site of Pisa-San Rossore, Italy: inferences on their provenance and possible trading routes, Archaeometry 49 (2007) 1–22.
[68] F. Marra, E. D'Ambrosio, Trace element classification diagrams of pyroclastic rocks from the volcanic districts of central Italy: the case study of the ancient roman ships of Pisa, Archaeometry 55 (6) (2013) 993–1019.
[69] F. Schön, T. Schäfer, J. Heinrichs, A. Gerdes, Hydraulische Zisternenverputze aus Karthago und Pantelleria (Italien), in: H. Dolenz, C. Flügel (Eds.), Römische und byzantinische Großbauten am Decumanus Maximus, von Zabern, Mainz, 2012, pp. 236–248.
[70] G. Rizzo, L. Ercoli, B. Megna, M. Parlapiano, Mortars from ancient and traditional water supply systems in Sicily, J. Therm. Anal. Calorim. 92 (1) (2008) 323–330.
[71] Ö. Cizer, K. Van Balen, D. Van Gemert, Competition between hydration and carbonation in hydraulic lime and lime-pozzolana mortars, Adv. Mater. Res. 133–134 (2010) 241–246.
[72] L.K. Davidson, T. Demeril, R.L. Handy, Soil pulverization and lime migration in soil lime stabilization, Highway Res. Record 92 (1965) 103–126.
[73] M.E. Karim, M.J. Alam, M.S. Hoque, Effect of salinity of water in lime-fly ash treated sand, Int. J. Geoeng. 8 (15) (2017).
[74] A. Meunier, Clays, Springer, Berlin, 2005.
[75] E. Bernard, B. Lothenbach, I. Pochard, C. Cau-Dit-Coumes, Alkali binding by magnesium silicate hydrates, J. Am. Ceram. Soc. (2019), http://dx.doi.org/10.1111/jace.16494.
[76] J. Bonetto, F. Ghedini, A.R. Ghiotto, Il foro di Nora. Le linee metodologiche della ricerca e lo scavo del tempio sul lato nord della piazza, in: Nora 2003. Atti della giornata di studi di Genova 6 maggio 2003, Servizio editoriale universitario di Pisa, Pisa, 2003, pp. 63–70.
[77] C. Previato, Nora. Le cave di pietra della città antica, Scavi di Nora, VI, Quasar edizioni, Roma, 2016.
[78] J. Bonetto, Nora da colonia cartaginese a municipio romano, in: S. De Vincenzo, C. Blasetti Fantauzzi (Eds.), Il processo di romanizzazione della provincia Sardinia et Corsica, Analysis Archaeologica. An International Journal of Western Mediterranean Archaeology, Monograph series 1, Edizioni Quasar, Roma, 2016, pp. 165–190.
[79] T. Zhang, C.R. Cheeseman, L.J. Vandeperre, Development of low pH cement systems forming magnesium silicate hydrate (M-S-H), Cem. Concr. Res. 41 (2011) 439–442.
[80] J. Szczerba, R. Prorok, E. Sniezek, D. Madej, K. Maslona, Influence of time and temperature on ageing and phases synthesis in the MgO, SiO_2, H_2O system, Thermochim. Acta 567 (2013) 57–64.
[81] Y. Zhang, Y. Li, Y. Xu, S. Sang, S. Jin, Enhanced formation of magnesium silica hydrates (M-S-H) using sodium metasilicate and caustic magnesia in magnesia castables, Ceram. Int. 43 (2017) 9110–9116.
[82] D. Nied, K. Enemark-Rasmussen, E. L'Hopital, J. Skibsted, B. Lothenbach, Properties of magnesium silicate hydrates (M-S-H), Cem. Concr. Res. 79 (2016) 323–332.
[83] C. Sonat, C. Unluer, Investigation on the performance and thermal decomposition of MgO and MgO-SiO_2 formulations, Thermochim. Acta 655 (2017) 251–261.
[84] H.M. Tran, A. Scott, Strength and workability of magnesium silicate hydrate binder systems, Constr. Build. Mater. 131 (2017) 526–535.
[85] C. Sonat, W.W. Teo, C. Unluer, Performance and microstructure of MgO-SiO2 concrete under different environments, Constr. Build. Mater. 184 (2018) 549–564.